

Online Similarity-and-Independence-Aware Beamformer for Low-latency Target Sound Extraction

Atsuo Hiroe, *Member, IEEE*

Abstract This study describes an online target sound extraction (TSE) process, derived from the iterative batch algorithm using the similarity-and-independence-aware beamformer (SIBF), to achieve both latency reduction and extraction accuracy maintenance. The SIBF is a linear method that estimates the target more accurately compared with a reference, an approximate magnitude spectrogram of the target. Evidently, deriving the online algorithm from the iterative batch algorithm reduces the latency of the SIBF; however, this process presents two challenges: 1) the derivation may degrade the accuracy, and 2) the conventional post-process, meant for scaling the estimated target, may increase the accuracy gap between the two algorithms. To maintain the best possible accuracy, herein, an approach that minimizes this gap during post-processing is adopted, and a novel scaling method based on the single-channel Wiener filter (SWF-based scaling) is proposed. To improve the accuracy further, the time–frequency-varying variance generalized Gaussian (TV GG) distribution is employed as a source model to represent the joint probability between the target and reference. Thus, experiments using the CHiME-3 dataset confirm that 1) the online algorithm reduces latency; 2) SWF-based scaling eliminates the gap between the two algorithms while improving the accuracy; 3) TV GG model achieves the best accuracy when it corresponds to the Laplacian model; and 4) our online SIBF outperforms the conventional linear TSE, including the minimum mean square error beamformer. These findings can contribute to the fields of beamforming and blind source separation.

Index Terms— target sound extraction, similarity-and-independence-aware beamformer, online algorithm, low latency, single-channel Wiener filter

I. INTRODUCTION

Target sound extraction (TSE) is the process of estimating a target (sound of interest) from one or more mixtures of multiple sound sources. It plays a crucial role in improving the speech intelligibility of humans and automatic speech recognition (ASR) by computers [1], [2]. The methods for TSE are generally classified as linear and nonlinear. Recently, nonlinear methods have significantly improved owing to the development of deep neural networks (DNNs). These DNN-based TSE methods can extract a clean speech from overlapping utterances of multiple speakers or a noisy source. Typically, these employ, as clues for the target, information, such as an enrollment speech, video of a human face, and text query [3]–[6]. By contrast, linear methods are advantageous in avoiding nonlinear distortions, such as musical noises and spectral distortions [7], [8]. Linear methods can be further categorized into two types: beamformers (BFs) using time–frequency (TF) masks, referred to as mask-based BFs [9]–[11]; and TSE methods based on the independent component analysis (ICA) [12], referred to as ICA-based TSE [13]–[16].

Adopting the ICA-based TSE, we previously developed a novel method called the *similarity-and-independence-aware beamformer* (SIBF) [17], [18]. The SIBF employs a magnitude spectrogram generated with any target-enhancing method, including the DNN-based TSE, as a reference for the target; its output is more accurate compared with the reference as it leverages the theory of the ICA. Considering that magnitude spectrograms can be obtained from various types of data, including waveforms and TF masks, the SIBF can be combined with different types of DNNs that output these data. Thus, one advantage of the SIBF is that it can be utilized to refine a DNN output.

Previously, we employed an iterative batch algorithm that simultaneously uses all the sound data included in a recorded segment, referred to as *batch SIBF*. However, in more practical scenarios, this algorithm suffers from the following issues.

- 1) The latency for obtaining the SIBF output becomes longer depending on the duration of the target [19] because the extraction process cannot start unless the recording of the target finishes. This implies that a downstream task, such as the ASR, experiences a latency longer than the sum of the recording and SIBF

TABLE I

SIGNAL NOTATIONS (VARIABLES f , t , AND k DENOTE THE INDICES OF THE FREQUENCY BIN, FRAME, AND CHANNEL, RESPECTIVELY; AND F , T , M , AND N DENOTE TOTAL NUMBERS OF FREQUENCY BINS, FRAMES, SOURCES AND MICROPHONES, RESPECTIVELY.)

Signal name	Spectrogram	An element	Column vector of all channel elements
Source	$\mathbf{S}_k \in \mathbb{C}^{F \times T}$	$s_k(f, t) \in \mathbb{C}$	$\mathbf{s}(f, t) = [s_1(f, t), \dots, s_M(f, t)]^T$
Observation	$\mathbf{X}_k \in \mathbb{C}^{F \times T}$	$x_k(f, t) \in \mathbb{C}$	$\mathbf{x}(f, t) = [x_1(f, t), \dots, x_N(f, t)]^T$
Estimated target	$\mathbf{Y} \in \mathbb{C}^{F \times T}$	$y(f, t) \in \mathbb{C}$	(Not available)
Reference	$\mathbf{R} \in \mathbb{R}^{F \times T}$	$r(f, t) \in \mathbb{R}$	(Not available)

processing times.

- Only a single filter is estimated in the segment. Thus, if the sources are nonstationary or moving, the extraction accuracy tends to be lower [20].

The present study focuses on the first issue, even though the employed approaches address both the issues. Thus, the goal of this study is to reduce the latency while maintaining the extraction accuracy, compared with the batch SIBF.

A possible solution to both the aforementioned issues involves updating the extraction filter, which generates the estimated target from the observations, at a short interval, for example, frame by frame. We refer to this method as the *online algorithm* (or *online SIBF* as needed). To this end, the following processes need to be online.

- Reference generation
- Filter estimation
- Pre-process and post-process

First, for reference generation, the framework of low-latency speech separation methods can be applied using convolutional neural networks (CNNs) [21] and long-short-term memories (LSTMs) [22]. Therefore, this study focuses on the remaining two processes.

Second, for filter estimation, the latency can be reduced by deriving the corresponding online algorithm from the iterative batch SIBF, by applying techniques employed in existing online TSE methods. However, as a side effect of the latency reduction, the derivation may degrade the extraction accuracy because it changes the dependencies between the extraction filter and related signals. This issue has not yet been investigated, although we anticipate that the ICA-based TSE approaches also most likely face the same issue.

Third, both online pre- and post-processes must be employed. The latter involves adjusting the scale of the estimated target. However, the conventional scaling method based on the minimal distortion principle [23] (MDP-based scaling) may increase the accuracy gap between the batch and online SIBFs because this method may estimate a less accurate scale as the extraction accuracy degrades. This issue has not yet been investigated properly.

To both reduce the latency and maintain the extraction accuracy, this study adopts an approach that minimizes this gap in post-process. Therefore, instead of the MDP-based scaling, this study proposes a novel scaling method that can estimate the scale of the estimated target more properly.

Furthermore, to improve the extraction accuracy, this study examines a source model that represents a joint probability between the target and reference. Previously, we examined three models, namely the time–frequency-varying

variance (TV) Gaussian, bivariate spherical (BS) Laplacian, and TV Student’s t (TV t) models. Compared with the TV Gaussian model, the other two can extract the target more accurately; however, they require iterative algorithms. Additionally, in the field of blind source separation (BSS), for example, the independent low-rank matrix analysis and nonnegative matrix factorization, the TV Gaussian model has been generalized to achieve a better accuracy [24]–[27]. We refer to this as the TV generalized Gaussian (TV GG) model. Considering that the TV GG model has similar characteristics as the BS Laplacian and TV t models, this study adapts this model to the SIBF framework and compares it with the aforementioned three models.

The remainder of this paper is organized as follows. Section II explains the formulation of the SIBF; Section III reviews the techniques employed in the linear TSE methods to derive the online SIBF; Section IV presents the stepwise derivation of the online algorithm for the SIBF and discusses the possible accuracy degradation; Section V discusses the online pre- and post-processes, including the proposed scaling method; Section VI reviews the existing source models and examines the TV GG model; Section VII conducts a sequence of experiments; Section VIII discusses the experimental results; finally, Section IX presents the conclusions of this study.

II. FORMULATION OF THE SIBF

Before delving into the derivation of the online SIBF, this section provides an updated formalization of the SIBF. This method was initially formulated in [17] as an extension of the deflationary ICA [12], then unified with the formulation of the mask-based BFs in [18]. This section explains the unified formulation.

The notations listed in Table I are used consistently throughout this paper to represent the TF domain signals, with f , t , and k denoting the indices of the frequency bin, frame, and channel, respectively. These indices begin with 1. Each spectrogram consists of F frequency bins and T frames. The estimated target after adjusting its scale is referred to as the *SIBF output* to be distinguished from \mathbf{Y} . Moreover, to emphasize the assignment to a variable, the left arrow ‘←’ is used instead of ‘=’ as needed.

Fig. 1 shows the workflow of the SIBF. The inputs are the multichannel observation spectrograms obtained from multiple microphones, and the output is a spectrogram of the estimated target. A magnitude spectrogram associated with the target is used as the reference, and can be estimated using various methods, including the DNN-based TSE. The

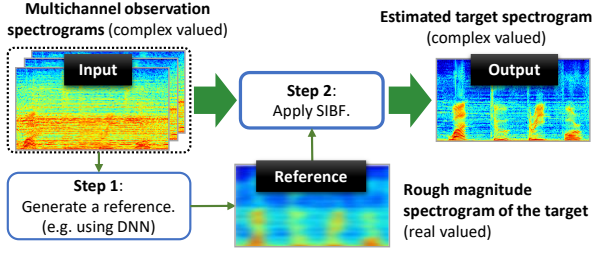


Fig. 1 Workflow of SIBF

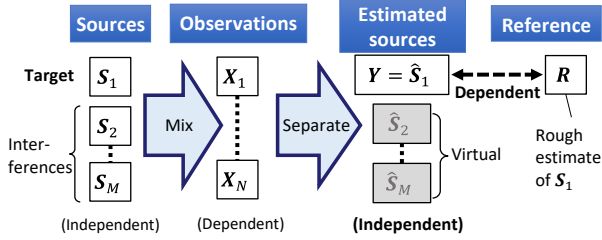


Fig. 2 Framework of SIBF

workflow involves two steps: 1) estimating the rough magnitude spectrogram of the target, and 2) applying the SIBF with the rough spectrogram as the reference.

A. Framework of the SIBF

Fig. 2 illustrates the framework of the SIBF, including the mixing and separating processes of the signals. Unlike our previous study [18], the decorrelation process is excluded. The framework assumes that M sources $\mathbf{S}_1, \dots, \mathbf{S}_M$ are mutually independent. Without loss of generality, \mathbf{S}_1 is considered the target source, namely the source of interest in this study, whereas the other sources are considered as interferences. The observations $\mathbf{X}_1, \dots, \mathbf{X}_N$ represent the spectrograms obtained from N microphones. In the TF domain, each observation spectrogram \mathbf{X}_k is approximated as an instantaneous mixture of sources. From the assumption of the sources, the estimated sources $\hat{\mathbf{S}}_1, \dots, \hat{\mathbf{S}}_M$ are also mutually independent. Considering that only $\hat{\mathbf{S}}_1$ is of interest, this is represented as \mathbf{Y} . To certainly associate \mathbf{Y} with the target source \mathbf{S}_1 , the dependence between \mathbf{Y} and the reference \mathbf{R} , as well as the independence of all the estimated sources, are leveraged. The objectives are to make \mathbf{Y} both similar to the reference using the dependence and more accurate than the reference using the independence. To generate only \mathbf{Y} , deflationary estimation [12], i.e., one-by-one separation, is employed. This indicates that the other estimated sources, $\hat{\mathbf{S}}_2, \dots, \hat{\mathbf{S}}_M$, are virtual. In each frequency bin, \mathbf{Y} is estimated as follows.

$$y(f, t) = \mathbf{w}(f)^H \mathbf{x}(f, t), \quad (1)$$

where $\mathbf{w}(f) \in \mathbb{C}^{N \times 1}$ is a filter that generates $y(f, t)$ from $\mathbf{x}(f, t)$. Herein, $\mathbf{w}(f)$ is referred to as the *extraction filter*.

B. Estimating the Extraction Filter

The target sound extraction problem, shown in Fig. 2, can be solved using maximum-likelihood (ML) estimation [28].

As derived in our previous study [18], $\mathbf{w}(f)$ can be formulated as the solution to the following constrained minimization problem.

$$\mathbf{w}(f) = \arg \min_{\mathbf{w}(f)} \left\{ - \sum_t \log p(r(f, t), y(f, t)) \right\}, \quad (2)$$

$$\text{s. t. } \frac{1}{T} \sum_t |y(f, t)|^2 = 1, \quad (3)$$

where $p(\cdot)$ denotes a *source model* that is a joint probability density function between the given reference and target used to represent the dependence between them. The constraint given by (3) helps avoid the trivial solution that $\mathbf{w}(f) = 0$.

Our previous study demonstrated that $\mathbf{w}(f)$ could be estimated as the eigenvector corresponding to the minimum eigenvalue in the following generalized eigenvalue (GEV) problem, and that the differences in the source models appear only in computing the weight $c(f, t)$.

$$\Phi_x(f) = \frac{1}{T} \sum_t \mathbf{x}(f, t) \mathbf{x}(f, t)^H, \quad (4)$$

$$\Phi_c(f) = \frac{1}{T} \sum_t c(f, t) \mathbf{x}(f, t) \mathbf{x}(f, t)^H, \quad (5)$$

$$\mathbf{w}(f) = \text{GEV}_{\min}(\Phi_c(f), \Phi_x(f)), \quad (6)$$

where $\Phi_x(f)$ and $\Phi_c(f)$ are referred to as the observation and weighted covariance matrices, respectively; and $\text{GEV}_{\min}(\mathbf{A}, \mathbf{B})$ denotes the eigenvector \mathbf{v} corresponding to the minimum eigenvalue λ_{\min} in the following GEV problem.

$$\mathbf{A}\mathbf{v} = \lambda_{\min} \mathbf{B}\mathbf{v}. \quad (7)$$

Our previous study [18] examined the TV Gaussian, TV t, and BS Laplacian models as candidates for the source models. The TV Gaussian model and corresponding weight are represented as (8) and (9), respectively.

$$p(r(f, t), y(f, t)) \propto \exp\left(-\frac{|y(f, t)|^2}{\max(r(f, t)^\beta, \varepsilon)}\right), \quad (8)$$

$$c(f, t) = \frac{1}{\max(r(f, t)^\beta, \varepsilon)}, \quad (9)$$

where $\max(\cdot)$ denotes selecting the maximum argument; β , referred to as the *reference exponent*, is a hyperparameter to control the influence of the reference; and ε , referred to as a *clipping threshold*, is a small positive value to avoid division by zero. Using (9), (5), (6), and (4), $\mathbf{w}(f)$ is obtained as the closed-form solution.

Additionally, The TV t and BS Laplacian models are described in (10) and (11), respectively.

$$p(r(f, t), y(f, t)) \propto \frac{1}{r(f, t)^2} \left(1 + \frac{2|y(f, t)|^2}{v r(f, t)^2} \right)^{-\frac{2+\nu}{2}}, \quad (10)$$

$$p(r(f, t), y(f, t)) \propto \exp\left(-\sqrt{\alpha r(f, t)^2 + |y(f, t)|^2}\right), \quad (11)$$

where ν and α , referred to as a *degree of freedom* and *reference weight*, respectively, are hyperparameters to control the influence of the reference. As both ν and α are sensitive to the scale of the reference, the square mean of the reference must be adjusted to one when the fixed ν and α are applied to various references; this process is called *reference normalization*. Although the two models do not have the closed-form solutions, the formulae for the weight $c(f, t)$ can be derived by applying the auxiliary function (or maximization–majorization) algorithm [29], [30], as follows.

$$c(f, t) = \frac{\nu + 2}{\nu r(f, t)^2 + 2|y(f, t)|^2}, \quad (12)$$

$$c(f, t) = \frac{1}{\sqrt{\alpha r(f, t)^2 + |y(f, t)|^2}}. \quad (13)$$

When utilizing the TV t model, (1), (12), (5), and (6) are iteratively employed to obtain $\mathbf{w}(f)$. Whereas when using the BS Laplacian model, (13) is employed, instead of (12). Although the first iteration requires computing $c(f, t)$ without $\mathbf{w}(f)$, the TV Gaussian model can be leveraged; essentially, (9) can replace (12) and (13). This methodology is referred to as the *boost start* [18].

Regarding the TV Gaussian model, there exist two possible interpretations of the term TV. Each study that utilizes this model, including [14], [31], and [32], adopts one of the following two interpretations:

- 1) In [32] and within the SIBF framework, the TV terms are predetermined and considered as constants. For instance, in this study, the TV terms correspond to the denominators in (8) and (9). This interpretation eliminates the need for an iterative process to determine $\mathbf{w}(f)$.
- 2) In [14] and [31], both the TV terms and the extraction filter are variables to be estimated. Such an interpretation necessitates an iterative algorithm that updates both sets of parameters in an alternating manner.

In this study, the second interpretation is treated as a particular case of the TV t model because the case of $\nu = 0$ makes (12) identical to (14), which regards $|y(f, t)|^2$ as an estimate of the TV and, hence, conforms to the second interpretation.

$$c(f, t) = \frac{1}{|y(f, t)|^2}. \quad (14)$$

III. RELATED WORK

This section discusses techniques used in the linear TSE methods to derive the online algorithm. The subsequent

subsections review two categories of methods, namely the mask-based BF and ICA-based TSE.

A. Online Mask-based BFs

Online algorithms have been proposed for the following mask-based BFs.

- 1) Maximum signal-to-noise ratio (max-SNR) or GEV BF [33]–[35];
- 2) Minimum variance distortionless response (MVDR) BF [20], [36]–[40];
- 3) Minimum mean square error (MMSE) or multichannel Wiener filter (MWF) BF [20], [41].

Although each BF method employs a different formula to estimate the extraction filter, common techniques are applied to derive the corresponding online algorithms.

The mask-based BFs use one or two weighted covariance matrices of the observations. In the batch algorithm, these matrices are computed from all the data included in the segment as illustrated in Fig. 3 (a). For estimating the extraction filter frame by frame, these matrices must be updated simultaneously. Let $\Phi_m(f, t)$ be a weighted covariance matrix computed at frame t . A sliding window enables to update $\Phi_m(f, t)$ frame by frame, as follows [42].

$$\Phi_m(f, t) = \frac{1}{T_b} \sum_{\tau=0}^{T_b-1} g^\tau m(f, t-\tau) \mathbf{x}(f, t-\tau) \mathbf{x}(f, t-\tau)^H, \quad (15)$$

where, T_b , g , and $m(f, t)$ denote the window length, a forgetting factor such that $0 < g < 1$, and a mask value for the target or interferences, respectively. This computation method is called *windowed batch*, and it is illustrated in Fig. 3 (b). This method is still treated as a batch algorithm.

The windowed batch algorithm can equivalently be described as (16) to reduce the computational cost [33], [42].

$$\Phi_m(f, t) = g\Phi_m(f, t-1) + (1-g)\{m(f, t)\mathbf{x}(f, t)\mathbf{x}(f, t)^H - g^{T_b}m(f, t-T_b)\mathbf{x}(f, t-T_b)\mathbf{x}(f, t-T_b)^H\}. \quad (16)$$

Considering that this computation can be performed using a first-in and first-out (FIFO) buffer, it is referred to as *FIFO online* and is shown in Fig. 3 (c).

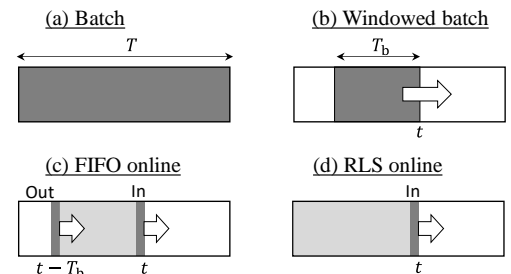


Fig. 3 Steps for the derivation of online algorithm from the batch algorithm to the online algorithm; (a) batch, (b) windowed batch, (c) FIFO online, and (d) RLS online algorithms

When T_b is sufficiently large, g^{T_b} is close to zero. Thus, (16) can be approximated as follows [43].

$$\Phi_m(f, t) = g\Phi_m(f, t-1) + (1-g)m(f, t)\mathbf{x}(f, t)\mathbf{x}(f, t)^H. \quad (17)$$

This algorithm is referred to as *recursive least square* (RLS) *online*, and is shown in Fig. 3 (d). This algorithm has been extensively used in online BFs as it does not require buffering the past observations and mask values.

To further reduce the computational cost, the following techniques are employed.

- In the MVDR and MMSE BFs, matrix inversion lemma (MIL) is applied to efficiently update the inverse of $\Phi_m(f, t)$ [44], [45]. MIL applies to not only the RLS online algorithm but also the FIFO online [33].
- In the max-SNR BF, an iterative method, referred to as the *power method* (PM), is applied to solve the GEV problem efficiently [46], [47].

B. Online ICA-based TSE

This category includes the independent vector extraction (IVE) [13], [16], [48], and maximum likelihood distortionless response (MLDR) [14], [31], as well as the SIBF. For both the IVE and MLDR, online algorithms have been proposed, as presented in Table II.

In this study, these methods are briefly reviewed. IVE is an extension of independent vector analysis (IVA) [49]–[52] to the problem of extracting a single source. To extract only the target, the IVE is further extended to leverage a pilot signal associated with the target [53], [54]. Unlike the reference for the SIBF, the pilot is shared in all the frequencies because the IVE framework assumes that all the frequency bins in the same spectrogram depend on one another. Analogous to the IVA, the IVE incorporates the auxiliary function algorithm [54], [55]. Initially, however, the IVE was formulated using the gradient algorithm [13], [16], [48].

The online variant of the IVE has been derived in [53] and [56]. These studies employed techniques akin to those used in online BFs within the context of the iterative batch process governed by the auxiliary function algorithm. Specifically, the RLS online algorithm was employed to update a weighted covariance matrix, while the MIL was invoked to efficiently calculate its inverse matrix.

By contrast, the MLDR is an extension of the MVDR. This assumes that the target follows the TV Gaussian model to maximize the likelihood of the BF outputs under the distortionless response constraint. This category also includes

TABLE II
CLASSIFICATION OF ICA-BASED TSE

Method	Constraint	Batch	Online
SIBF	Unit variance	[17], [18]	This study
IVE	Dependence of all bins	[13], [16], [48]	[53], [56]
MLDR & WPD	Distortionless response	[15], [57]	[15], [31]

studies on the weighted power minimization distortionless response (WPD) [15], [57], because the WPD is interpreted as an integration of the MLDR and dereverberation [31]. Both the MLDR and WPD use an iterative algorithm that alternatively estimates the extraction filter and TV. As mentioned in Section II.B, this study treats this algorithm as a particular case of the TV t model rather than of the TV Gaussian model. To estimate only the target, these methods employ a steering vector corresponding to the direction of the target.

The online algorithms of the MLDR and WPD were derived in [31] and [15], respectively. Similar to the online IVE, the RLS online algorithm and MIL were applied in the derivation. The PM was also applied to solve the GEV problem used to estimate the steering vector.

Note that neither of the online IVE and MLDR approaches employs an iterative algorithm, although the corresponding batch algorithms are based on iterative algorithms. However, the side effects of omitting the iterations have not been investigated.

IV. DERIVATION OF ONLINE ALGORITHM FOR THE SIBF

In this section, the algorithm of the online SIBF is derived in a stepwise manner by applying the derivation techniques used in the online mask-based BF and ICA-based TSE.

A. Windowed Batch

Initially, the covariance matrices calculated using (4) and (5) are modified to facilitate frame-by-frame updates. Let $\Phi_x(f, t)$ and $\Phi_c(f, t)$ be the observation and weighted covariance matrices in the t -th frame, respectively. In the windowed batch algorithm illustrated in Fig. 3 (b), both matrices can be computed, as shown in (18) and (19).

$$\Phi_x(f, t) = (1-g) \sum_{\tau=0}^{T_b-1} g^\tau \mathbf{x}(f, t-\tau)\mathbf{x}(f, t-\tau)^H, \quad (18)$$

$$\Phi_c(f, t) = (1-g) \sum_{\tau=0}^{T_b-1} g^\tau c(f, t-\tau)\mathbf{x}(f, t-\tau)\mathbf{x}(f, t-\tau)^H, \quad (19)$$

where $c(f, t-\tau)$ is computed, for $0 \leq \tau < T_b$, from (9), (12), or (13) depending on the source model employed. Let $\mathbf{w}(f, t)$ be the extraction filter estimated in the t -th frame. Similar to the batch SIBF, $\mathbf{w}(f, t)$ can be computed as follows.

$$\mathbf{w}(f, t) = \text{GEV}_{\min}(\Phi_c(f, t), \Phi_x(f, t)). \quad (20)$$

When (12) and (13) are used, the estimated target $y(f, t-\tau)$, included in $c(f, t-\tau)$, can be computed as follows.

$$y(f, t-\tau) = \mathbf{w}(f, t)^H \mathbf{x}(f, t-\tau). \quad (21)$$

Both (19) and (21) indicate that $c(f, t-\tau)$ for $0 \leq \tau < T_b$ needs to be computed whenever $\mathbf{w}(f, t)$ is updated. This

characteristic applies to the ICA-based TSE and differs from that of the mask-based BF.

In the case of $1 \leq t < T_b$, the value of $t - \tau$ can be zero or negative. To compute the covariance matrices in (18) and (19), the observation and reference when the frame index is zero or negative are defined as follows.

$$\mathbf{x}(f, -\tau) = \mathbf{x}(f, T_b - \tau), \quad (22)$$

$$r(f, -\tau) = r(f, T_b - \tau), \quad (23)$$

where $0 \leq \tau < T_b$. Note that these definitions introduce a latency of T_b frames, whereas the covariance matrices can be computed in a stable manner.

B. FIFO Online

To reduce the computational cost, the FIFO online algorithm illustrated in Fig. 3 (c) is derived. Herein, $\Phi_x(f, t)$ can be described as (24), which is equivalent to (18).

$$\Phi_x(f, t) = g\Phi_x(f, t-1) + (1-g)\{\mathbf{x}(f, t)\mathbf{x}(f, t)^H - g^{T_b}\mathbf{x}(f, t-T_b)\mathbf{x}(f, t-T_b)^H\}. \quad (24)$$

By contrast, $\Phi_c(f, t)$ cannot be described as an equivalent formula in the same manner as FIFO online because $c(f, t - \tau)$ needs to be updated depending on $\mathbf{w}(f, t)$, as mentioned in Section IV.A. However, if (25) is employed instead of (21), $\Phi_c(f, t)$ can be approximately described, as shown in (26).

$$y(f, t - \tau) = \mathbf{w}(f, t - \tau)^H \mathbf{x}(f, t - \tau), \quad (25)$$

$$\Phi_c(f, t) = g\Phi_c(f, t-1) + (1-g)\{c(f, t)\mathbf{x}(f, t)\mathbf{x}(f, t)^H - g^{T_b}c(f, t-T_b)\mathbf{x}(f, t-T_b)\mathbf{x}(f, t-T_b)^H\}. \quad (26)$$

Note that (26) is no longer equivalent to (19) when using a source model other than the TV Gaussian model. This may cause side effects, such as accuracy degradation.

C. RLS Online

Similar to the existing online BFs, formulae for the RLS online algorithm can be derived, as shown in Fig. 3 (d). Given that g^{T_b} is close to zero when T_b is sufficiently large, (24) and (26) can be approximated as (27) and (28), respectively.

$$\Phi_x(f, t) = g\Phi_x(f, t-1) + (1-g)\mathbf{x}(f, t)\mathbf{x}(f, t)^H, \quad (27)$$

$$\Phi_c(f, t) = g\Phi_c(f, t-1) + (1-g)c(f, t)\mathbf{x}(f, t)\mathbf{x}(f, t)^H. \quad (28)$$

Here, we describe how to compute the initial values in (27) and (28), such as $\Phi_x(f, 0)$ and $\Phi_c(f, 0)$, respectively. Several studies employing the RLS online algorithm report that the initial values of the covariance matrices affect the extraction accuracy [39], [40]. In this study, the initial values are

computed with the windowed batch algorithm. Considering that T_b is used only once, this is referred to as the *initial batch duration*.

Note that the RLS online algorithm experiences the same side effects from employing (25), because this approximates the FIFO online algorithm.

D. Computational Reduction in the Filter Estimation

The computational cost in obtaining $w(f, t)$ computed in (20) should be reduced. To solve the GEV problem in (20) more efficiently, the PM is applied in the same manner as in the max-SNR BF [46], [47], [58]. Originally, the PM solves the standard eigenvector (SEV) problem, expressed as (29).

$$\mathbf{A}\mathbf{v} = \lambda_{\max}\mathbf{v}, \quad (29)$$

where \mathbf{A} , λ_{\max} , and \mathbf{v} denote a square matrix, its maximum eigenvalue, and the corresponding eigenvector, respectively. This method performs (30) and (31) alternately until \mathbf{v} converges.

$$\mathbf{v} \leftarrow \mathbf{A}\mathbf{v}, \quad (30)$$

$$\mathbf{v} \leftarrow \frac{\mathbf{v}}{\sqrt{\mathbf{v}^H\mathbf{v}}} \quad (31)$$

Employing (31) can prevent \mathbf{v} from diverging or converging to the zero vector.

To apply the PM to the SIBF, (20) and (7), which represent the GEV problem using the minimum eigenvalue, can be rewritten as (32), which represents the SEV [46].

$$\Phi_c(f, t)^{-1}\Phi_x(f, t)\mathbf{w}(f, t) = \frac{1}{\lambda_{\min}(f, t)}\mathbf{w}(f, t). \quad (32)$$

By applying (30) to (32), we obtain (33). To satisfy (3), (34) is used, instead of directly applying (31).

$$\mathbf{w}(f, t) \leftarrow \frac{\Phi_c(f, t)^{-1}\Phi_x(f, t)\mathbf{w}(f, t)}{\mathbf{w}(f, t)}, \quad (33)$$

$$\mathbf{w}(f, t) \leftarrow \frac{\mathbf{w}(f, t)}{\sqrt{\mathbf{w}(f, t)^H\Phi_x(f, t)\mathbf{w}(f, t)}} \quad (34)$$

As mentioned in Section III.A, the MIL allows us to efficiently compute the matrix inversion included in (33). The MIL is written as follows [44], [45].

$$(\mathbf{A} + d\mathbf{b}\mathbf{b}^H)^{-1} = \mathbf{A}^{-1} - \frac{\mathbf{A}^{-1}\mathbf{b}\mathbf{b}^H\mathbf{A}^{-1}}{1/d + \mathbf{b}^H\mathbf{A}^{-1}\mathbf{b}}, \quad (35)$$

where \mathbf{A} , \mathbf{b} , and d denote an $N \times N$ full-rank matrix, $N \times 1$ vector, and a scalar value, respectively. To compute $\Phi_c(f, t)^{-1}$ efficiently, the MIL can be fit to (28) through the following assignments.

$$\mathbf{A} = g\Phi_c(f, t-1), \quad (36)$$

$$\mathbf{A}^{-1} = \frac{1}{g} \Phi_c(f, t-1)^{-1}, \quad (37)$$

$$\mathbf{b} = \mathbf{x}(f, t), \quad (38)$$

$$d = (1-g)c(f, t). \quad (39)$$

Algorithm 1 presents the pseudocode for the RLS online algorithm with the PM and MIL. Lines ending with ‘(*1)’ are skipped when using the TV Gaussian model. The frequency index ‘*’ indicates all the frequency bins. For example, Line 3 indicates that $\mathbf{x}(1, t)$ to $\mathbf{x}(F, t)$ are computed and buffered.

In Line 1, $\min(\cdot)$ indicates selecting the minimum value of the arguments. This line supports the case that the segment duration is smaller than the initial batch duration T_b . Even in the case, this algorithm updates $\mathbf{w}(*, t)$ frame by frame. Lines 2–5 prepare the observations and references when the frame index is zero or negative, as shown in (22) and (23). Computing $\mathbf{x}(*, t)$ includes both capturing proper duration of multichannel sound data from an audio device and applying the short-time Fourier transform (STFT) to these data. To buffer both $\mathbf{x}(*, t)$ and $r(*, t)$, the FIFO buffer that can store the data of T_b frames is used. Line 6 computes the initial values for pre- and post-processes mentioned in Section V.

Algorithm 1: RLS online algorithm with PM and MIL

```

1:  $T_b \leftarrow \min(T_b, T)$ 
2: for  $t = 1$  to  $T_b$  do
3:   Compute and buffer  $\mathbf{x}(*, t)$ .
4:   Compute and buffer  $r(*, t)$ .
5: end for
6: Compute the initial values for pre- and post-
   processes.
7: Compute  $\Phi_x(*, 0)$  using (18) with  $t = 0$ .
8: Compute  $\mathbf{w}(*, 0)$  using TV Gaussian model.
9: Compute  $\Phi_c(*, 0)$  using (19) with  $t = 0$  and its
   inverse.
10: for  $t = 1$  to  $T$  do
11:   if  $t > T_b$  then
12:     Compute  $\mathbf{x}(*, t)$ .
13:     Compute  $r(*, t)$ .
14:   end if
15:   Normalize  $r(*, t)$  using (41) and (42).
16:   Update  $\Phi_x(*, t)$  using (27).
17:    $\mathbf{w}(*, t) \leftarrow \mathbf{w}(*, t-1)$ 
18:   for  $i = 1$  to  $K_{\text{aux}}$  do (*1)
19:     Compute  $y(*, t)$  using (25) with  $\tau = 0$  (*1).
20:     Compute  $c(*, t)$  depending on the source
       model used.
21:     Update  $\Phi_c(*, t)^{-1}$  using the MIL.
22:     for  $j = 1$  to  $K_{\text{pm}}$  do
23:       Update  $\mathbf{w}(*, t)$  using (33) and (34).
24:     end for
25:   end for (*1)
26:   Compute  $y(*, t)$  using (25) with  $\tau = 0$ .
27:   Adjust the scale of  $y(*, t)$ .
28: end for

```

(*1) This line is skipped when the TV Gaussian model is used.

Lines 7–9 prepare the initial values of the covariance matrices and extraction filter. These are computed with the windowed batch algorithm, as mentioned in Section IV.A. Line 8 obtains the initial filter $\mathbf{w}(*, 0)$ using the TV Gaussian model, even when other models are used in the rest of the process. Line 9 computes $c(*, -\tau)$ for $0 \leq \tau < T_b$ to compute $\Phi_c(*, 0)$, depending on the source model. When using source models other than the TV Gaussian model, Line 9 first computes $y(*, -\tau)$ using (21) with $t = 0$ to obtain $c(*, -\tau)$.

The rest of the lines represent the process for each frame. In Lines 12 and 13, neither $\mathbf{x}(*, t)$ nor $r(*, t)$ need to be buffered in the RLS online algorithm. The normalization process in Line 15 is explained in Section V.A. Lines 18–25 indicate the loop of K_{aux} iterations for estimating $\mathbf{w}(*, t)$ based on the auxiliary function algorithm. These lines are not iterated in the TV Gaussian case. Note that this study leaves this loop to evaluate its effect, whereas the conventional ICA-based online TSE methods omitted this [15], [31], [53], [56]. Line 21 computes the inverse of $\Phi_c(*, t)$ using the MIL. Lines 22–24 represent the K_{pm} iterations based on the PM to estimate $\mathbf{w}(*, t)$.

Lines 26 and 27 generate the SIBF output in the frame t . The scaling method in Line 27 is explained in Section V.B.

V. ONLINE PRE- AND POST-PROCESSES

Given that the online system requires that both pre- and post-processes also be online, the processes are derived based on the RLS online algorithm. Unlike the filter estimation, the FIFO online algorithm is equivalent to the windowed batch algorithm. Therefore, the RLS online algorithm can approximate both the algorithms.

A. Reference Normalization as Pre-process

Pre-process includes the reference normalization mentioned in Section II.B. Based on the RLS online algorithm, this process can be described as follows.

$$v_{\text{ref}}(f, 0) = (1-g) \sum_{\tau=0}^{T_b-1} g^\tau r(f, -\tau)^2, \quad (40)$$

$$v_{\text{ref}}(f, t) = g v_{\text{ref}}(f, t-1) + (1-g) r(f, t)^2, \quad (41)$$

$$r_{\text{norm}}(f, t) = \frac{r(f, t)}{\sqrt{v_{\text{ref}}(f, t)}}, \quad (42)$$

where $v_{\text{ref}}(f, t)$ and $r_{\text{norm}}(f, t)$ denote the square mean of the reference and normalized reference, respectively. In Algorithm 1, Lines 9 and 20 use $r_{\text{norm}}(f, t)$ instead of $r(f, t)$.

B. Scaling as Post-process

In the SIBF framework, the scale of the estimated target is constrained with (3) during the filter estimation. Thus, it must be adjusted properly in post-process; this adjustment process is called *scaling*. Previously, we employed the MDP-based scaling [23], which has been extensively used in the ICA-based TSE and BSS fields. However, we found that this

method may estimate the scale inaccurately when the extraction is imperfect, as explained below. This subsection first explains a possible issue related to the MDP-based scaling, and then introduces a novel method that leverages the reference to avoid the issue.

1) Possible Issues with MDP-based Scaling

The MDP-based scaling is formulated as follows [23].

$$\gamma(f) = \arg \min_{\gamma(f)} \sum_t |x_m(f, t) - \gamma(f)y(f, t)|^2, \quad (43)$$

$$y_{\text{scale}}(f, t) = \gamma(f)y(f, t), \quad (44)$$

where $\gamma(f)$, $x_m(f, t)$, and $y_{\text{scale}}(f, t)$ denote the scaling factor, observation obtained with the m -th microphone, and SIBF output, respectively. Considering (3), $\gamma(f)$ can be computed as follows.

$$\gamma(f) = \frac{1}{T} \sum_t x_m(f, t) \overline{y(f, t)}, \quad (45)$$

where $\overline{y(f, t)}$ denotes the conjugate of $y(f, t)$.

To consider possible issues with the MDP-based scaling, we conceptually decompose the signals. For example, $x_m(f, t)$ and $y(f, t)$ are decomposed into two components as follows.

$$x_m(f, t) = x_{\text{tgt}}(f, t) + x_{\text{itf}}(f, t), \quad (46)$$

$$y(f, t) = y_{\text{tgt}}(f, t) + y_{\text{itf}}(f, t), \quad (47)$$

where $x_{\text{tgt}}(f, t)$ and $y_{\text{tgt}}(f, t)$ denote the components corresponding to the target, whereas $x_{\text{itf}}(f, t)$ and $y_{\text{itf}}(f, t)$ denote those corresponding to the other sources that are interferences. Herein, $y_{\text{itf}}(f, t)$ is considered as the *residual interferences*. From the independence assumption mentioned in Section II.A, the covariances between $x_{\text{tgt}}(f, t)$ and $y_{\text{itf}}(f, t)$, and between $y_{\text{tgt}}(f, t)$ and $x_{\text{itf}}(f, t)$ are considered to be 0. Thus, $\gamma(f)$ is conceptually identical to (48).

$$\gamma(f) = \frac{1}{T} \sum_t x_{\text{tgt}}(f, t) \overline{y_{\text{tgt}}(f, t)} + \frac{1}{T} \sum_t x_{\text{itf}}(f, t) \overline{y_{\text{itf}}(f, t)}. \quad (48)$$

The objective of the MDP-based scaling is to render the scale of $y(f, t)$ close to that of $x_{\text{tgt}}(f, t)$ using $x_m(f, t)$ [23]. If the extraction is perfectly executed, that is, $y_{\text{itf}}(f, t) = 0$, then (48) satisfies the objective. However, if $y_{\text{itf}}(f, t)$ persists, this formula tends to estimate an inaccurate scale due to the second term in (48).

This issue can be more critical for the online algorithm, as it may cause accuracy degradation, as mentioned in Section IV.B. Essentially, this method may increase the accuracy gap between the batch and online algorithms because $y_{\text{itf}}(f, t)$

may remain more loudly in the latter algorithm. Therefore, to minimize this gap, a different scaling method is required.

2) Proposed Scaling Method

To estimate the scale more accurately, this study proposes a novel scaling method based on the single-channel Wiener filter (SWF-based scaling) [59]–[61]. To be applied to the scaling problem, the SWF is formulated as the minimization problem described as (49) and compute its solution as given by (50).

$$\gamma(f) = \arg \min_{\gamma(f)} \sum_t |q(f, t) - \gamma(f)y(f, t)|^2 \quad (49)$$

$$= \frac{1}{T} \sum_t q(f, t) \overline{y(f, t)}, \quad (50)$$

where a complex number $q(f, t)$ denotes a reference signal for the scaling, referred to as the *scaling target*. Unlike in the original SWF, $\gamma(f)$ is applied to the estimated target $y(f, t)$ instead of the observation $x_m(f, t)$. This method, similar to the MDP-based scaling, is linear because this multiplies $y(f, t)$ only by a time-invariant value.

The ideal candidate of the scaling target is $x_{\text{tgt}}(f, t)$ described in (46) because $\gamma(f)$ can be described as (51) and is not disturbed by $x_{\text{itf}}(f, t)$ or $y_{\text{itf}}(f, t)$ unlike (48).

$$\gamma_{\text{ideal}}(f) = \frac{1}{T} \sum_t x_{\text{tgt}}(f, t) \overline{y_{\text{tgt}}(f, t)}, \quad (51)$$

where $\gamma_{\text{ideal}}(f)$ denotes the ideal scaling factor. Scaling using $\gamma_{\text{ideal}}(f)$ is referred to as *ideal scaling*. As $x_{\text{tgt}}(f, t)$ is not known in practical scenarios, an approximated value is used instead.

In this study, the following scaling target, which leverages $r(f, t)$, is used.

$$q(f, t) = r(f, t) \frac{x_m(f, t)}{|x_m(f, t)|}, \quad (52)$$

where $q(f, t)$ can be regarded as the combination of the reference for the SIBF and phase of the observation. If $q(f, t)$ is much closer to $x_{\text{tgt}}(f, t)$ than $x_m(f, t)$, the SWF-based scaling can approximately behave as the ideal scaling compared with the MDP-based scaling. Therefore, this method is able to not only avoid increasing the accuracy gap between the batch and online algorithms but also minimize it.

In the RLS online algorithm, the scaling factor can be computed as follows.

$$\boldsymbol{\varphi}_q(f, 0) = (1 - g) \sum_{\tau=0}^{T_b-1} g^\tau \mathbf{x}(f, t) \overline{q(f, -\tau)}, \quad (53)$$

$$\boldsymbol{\varphi}_q(f, t) = g \boldsymbol{\varphi}_q(f, t-1) + (1 - g) \mathbf{x}(f, t) \overline{q(f, t)}, \quad (54)$$

$$\gamma(f, t) = \boldsymbol{\varphi}_q(f, t)^H \mathbf{w}(f, t), \quad (55)$$

where $\gamma(f, t)$ and $\boldsymbol{\varphi}_q(f, t)$ denote the scaling factors in the t -th frame, and covariance vector between $\mathbf{x}(f, t)$ and $q(f, t)$, respectively.

Additionally, the RLS online algorithm for the MDP-based scaling can be obtained only by replacing $q(f, t)$ with $x_m(f, t)$ in (53) and (54). This indicates that the SWF-based scaling does not increase the computational cost compared with the MDP-based scaling.

VI. SOURCE MODELS

This section examines source models. First, an overview of the three models employed in our previous studies are presented; then, the TV GG model is examined.

A. Overview of the Existing Source Models

As mentioned in Section II.B, our previous study examined the TV Gaussian, BS Laplacian, and TV t models. Compared with the TV Gaussian model, the other two have similar characteristics, as described below:

- 1) Estimating the extraction filter requires an iterative algorithm based on the auxiliary function algorithm.
- 2) Both models outperform the TV Gaussian model in terms of the extraction accuracy.
- 3) The accuracy is sensitive to the scale of the reference.

Owing to the third aspect, both models practically require reference normalization.

The TV Gaussian model has contrasting characteristics compared with those of the other two. The extraction filter can be obtained without an iteration. This characteristic can be utilized to obtain the initial filter for the other models. While this model is robust to the scale of the reference, it is sensitive to the reference exponent β in (8) and exhibits two peaks in extraction accuracy when β is varied. Our previous study observed two peaks caused by the fact that the reference was powered before being clipped; one peak was obtained because a larger β brought $c(f, t)$ closer to a binary value in (9), whereas the other was unexpectedly caused by the fact that varying β changed the possibility of the clipping even if the clipping threshold ε was constant. Given that the latter peak was not optimal for tuning β , this model must be revised.

B. TV Generalized Gaussian Model

In the BSS field, the TV GG model, which is the generalized form of the TV Gaussian model, has been employed to achieve better separation accuracy [24]–[26]. In this study, this model is applied to the SIBF and compared with the existing three models.

Reflecting the overview in Section VI.A, we present a formula for the TV GG model as follows.

$$P(r(f, t), y(f, t)) \propto \exp\left(-\left(\frac{|y(f, t)|}{r'(f, t)^\beta}\right)^\rho\right), \quad (56)$$

where a positive value ρ , referred to as the *shape parameter*, determines the shape of the distribution, and $r'(f, t)$ denotes the clipped reference calculated as shown in (57).

$$r'(f, t) = \max(r(f, t), \varepsilon). \quad (57)$$

Compared with the original formula [24]–[26], (56) is unique in the following aspects.

- 1) The shape parameter ρ is applied to the denominator as well as to the numerator.
- 2) The denominator contains the reference exponent β to control the influence of the reference.
- 3) Opposite to (8), the reference is clipped before being powered. We expect that this can prevent two accuracy peaks appearing when β is varied.

For simplicity, this study focuses on the case of $0 < \rho \leq 2$. The cases of $\rho = 2$ and 1 are called the TV Gaussian and Laplacian models, respectively. In the TV Gaussian case, $\mathbf{w}(f)$ can be obtained using (4), (58), (5), and (6).

$$c(f, t) = \frac{1}{r'(f, t)^{2\beta}}. \quad (58)$$

Note that (58) is not identical to (8) owing to aspects 1) and 3) mentioned above. Similarly, $\mathbf{w}(f, t)$ for the RLS online algorithm can be obtained using (27), (58), (28), and (32) with the PM and MIL as mentioned in Section IV.D.

Conversely, when $\rho < 2$, the extraction filter lacks a closed-form solution. In this case, iterative rules may be formulated utilizing the auxiliary function algorithm [29], [30]. After substituting (56) into (2), the following inequality is obtained [24]:

$$\left(\frac{|y(f, t)|}{r'(f, t)^\beta}\right)^\rho \leq \frac{\rho|y(f, t)|^2}{2b(f, t)^{2-\rho}r'(f, t)^{2\beta}} + \left(1 - \frac{\rho}{2}\right)b(f, t)^\rho, \quad (59)$$

where $b(f, t)$ denotes a positive value referred to as the *auxiliary variable*. Differing from the original inequality used in [24], (59) includes the term $r'(f, t)^\beta$ in the denominator. The right-hand side in (59) is minimized and equal to the left-hand side when $b(f, t)$ satisfies (60).

$$b(f, t) = \frac{|y(f, t)|}{r'(f, t)^\beta}. \quad (60)$$

By employing (59) and (60), the weight $c(f, t)$ in (5) and (28) can be computed as follows.

$$c(f, t) = \frac{1}{r'(f, t)^{\beta\rho}|y(f, t)|^{2-\rho}}. \quad (61)$$

In the batch algorithm, $\mathbf{w}(f)$ can be obtained by using (1), (61), (5), and (6) iteratively, while the first iteration employs

the TV Gaussian model for the boost start. In the RLS online algorithm, $\mathbf{w}(f, t)$ can be obtained by using (25), (61), and (32) with the PM and MIL as mentioned in Section IV.D.

In addition, we can find that the case of $\rho = 0$ makes (61) identical to (14), which is regarded as a particular case of the TV t model in Section II.B. This indicates that the source model employed in [14] and [31] can be interpreted as particular cases of both the TV t and GG models rather than the TV Gaussian model.

VII. EXPERIMENTS

To verify whether the online SIBF can reduce the latency while maintaining the extraction accuracy, we conducted a series of experiments using the CHiME-3 dataset [1]. In this section, the term ‘‘online algorithm’’ essentially refers to the RLS online method, and the initial batch duration T_b is expressed in seconds.

The experiments consisted of the following steps:

- 1) Tuning the hyperparameters in the batch SIBF;
- 2) Comparing all the source models in the online SIBF;
- 3) Examining the iteration effects;
- 4) Comparing two scaling methods: the MDP- and SWF-based;
- 5) Measuring the latencies for the batch and online SIBFs;
- 6) Comparing the results obtained using the CHiME-3 simulated test set with those of the conventional methods.

We first explain the common experimental setup, and then demonstrate the results of each experiment sequentially.

A. Experimental Setup

1) Dataset

The CHiME-3 dataset contains sound data recorded in four noisy environments using six microphones attached to a tablet device and a clean speech recorded in a recording booth. The use of this dataset means that the SIBF is applied to a denoising task, in which speech is extracted from mixtures of speech and background noise.

To prepare the input data as a development set with various signal-to-noise ratios (SNRs), we artificially mixed the clean speech with a background (BG) noise. The clean speech consisted of 410 utterances from four speakers, which were recorded in a booth using six microphones attached to a tablet device. This dataset is labeled as *dt05_bth*. Background noises were recorded with the same device in four noisy environments such as a bus, caf e, pedestrian area, and street junction. During the mixing, we applied four multipliers (0.25, 0.5, 1.0, and 2.0) to the noises to represent the four scenarios shown in Table III. Each scenario consists of 1640 utterances.

In Section VII.G, we introduced another dataset called *CHiME-3 simulated test set*, used for comparing the SIBF with other methods. This consists of 1320 utterances that are a combination of 330 utterances from four speakers and four background noises.

TABLE III
FOUR SCENARIOS USED AS THE DEVELOPMENT SET

Scenario name	Relative noise level	Multiplier to BG	SNR [dB]
BG×0.25	Least noisy	0.25	14.05
BG×0.5	Less noisy	0.5	8.03
BG×1.0	Noisier	1.0	2.03
BG×2.0	Noisiest	2.0	-3.93

TABLE IV
STATISTIC DATA FOR EACH DATASET (Dev.: Development, Std.: Standard deviation)

Dataset	Number of utterances	Shortest [s]	Longest [s]	Mean [s]	Std. [s]
Dev.	1640	1.81	14.18	6.36	2.31
Test	1320	1.55	12.37	6.23	2.32

Table IV shows the number and durations of the utterances for each dataset.

2) Experimental System

Fig. 4 illustrates the experimental system employed in this study. The bold and thin lines denote the flows of multichannel and single-channel data, respectively. The index pair ‘ (f, t) ’ is omitted for simpler notation. The multichannel observations in the time-domain were converted to multichannel spectrograms by applying the STFT with 1024 points (640 ms) and 256 shifts (160 ms). As explained in Section VII.A.3), the reference was generated with the DNN from $x_5(f, t)$. Given that the fifth microphone was closest to the speaker position, the setting of $m = 5$ was also used in (45) and (52). This system can switch the scaling method between the MDP- and SWF-based methods.

The SIBF output $y_{\text{scale}}(f, t)$ was converted to the waveform by applying the inverse STFT (ISTFT) after replacing the frequency bin data under 62.5 Hz and over 7812.5 Hz with zeros. For evaluating the reference, $q(f, t)$ in (52) was also converted to the waveform.

We implemented the system in Python and utilized NumPy for matrix operation. The program was executed on a Linux PC with an Intel Core i7-7700K 4.2-GHz CPU and 32-GB RAM.

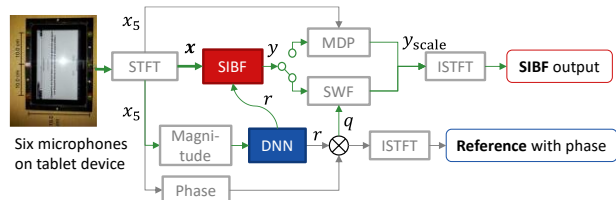


Fig. 4 Evaluation scheme for SIBF using CHiME-3 dataset

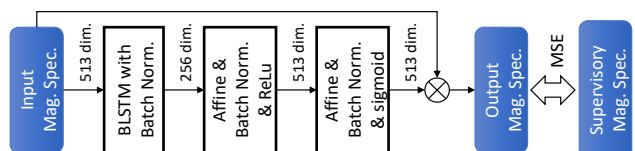


Fig. 5 DNN configuration that outputs a magnitude spectrogram (Mag. Spec.) as the reference. The numbers indicate the input and output dimensions.

TABLE V
EXPERIMENTAL SETUP EXPLAINED IN DIFFERENT SUBSECTIONS

Subsection	Algorithm	T_b [s]	Source model	Scaling	Dataset	Metric
VII.B	Batch	None	All	MDP	Development	Mean Δ SDR over four scenarios
VII.C	Online	1–5				
VII.D		2	TV Laplacian			
VII.E	Online & Batch	Online: 2, Batch: none		MDP & SWF	Test	Δ SDR for each scenario
VII.F			SWF	Latency in second		
VII.G					PESQ, SDR, STOI, eSTOI	

In this system, only the reference generation process using the DNN remained in the batch mode. Therefore, in the experiments for the online algorithm, we first computed and stored the references for all the frames, and then used the stored one in Lines 4 and 13 of Algorithm 1.

3) DNN Configuration

Fig. 5 illustrates the DNN configuration used for reference generation. Both the input and output of the DNN consisted of magnitude spectrograms. The network was trained to extract a singular speech source from a composite of clean speech and background noise. Owing to the inclusion of a bidirectional LSTM layer within the network architecture, the inference process operated in the batch mode.

B. Hyperparameter Tuning in Batch SIBF

Before evaluating the online SIBF, we confirmed the performance of the batch SIBF by tuning the hyperparameters of the TV GG model. The experimental setup is described in the first row of Table V. As a metric that represents the extraction accuracy, we used the signal-to-distortion ratio (SDR) [62]. We denote the difference between the SDR of the estimated target and that of the observation by Δ SDR.

The experiments for the batch algorithm consisted of three steps. First, we fixed ρ in (56) to 2 and explored the optimal β and ε as detailed in Appendix A. Consequently, we adopted $\beta = 1/4$ and $\varepsilon = 10^{-9}$ as the optimal hyperparameters for $\rho = 2$. In this section, we particularly refer to the TV GG model with these settings as the TV Gaussian model. These settings were also used for other models to obtain the initial value of the extraction filter.

TABLE VI
 Δ SDR FOR EACH SOURCE MODEL IN BATCH SIBF (the larger the better)

Source model	Hyperparameters			Δ SDR [dB]
	Iteration	ρ	Others	
TV Gaussian	None	2	$\beta = 1/4,$	5.70
TV Laplacian	10	1	$\varepsilon = 10^{-9}$	6.53
BS Laplacian		None	$\alpha = 100$	6.05
TV t			$\nu = 1$	6.35

TABLE VII
HYPERPARAMETERS ADOPTED IN RLS ONLINE WITH PM

Name	Value	Reason
Forgetting factor	$g = 0.99$	This shows the best Δ SDR among 0.95, 0.98, and 0.99.
Iteration count for PM	$K_{pm} = 2$	When $K_{pm} \geq 2$, Δ SDR converges to the value almost same as that using the GEV.

Next, we varied ρ and β , while fixing ε as described in Appendix B, and adopted $\rho = 1$ and $\beta = 1/4$ as the optimal values. We particularly refer to the TV GG model with these settings as the TV Laplacian model.

Finally, we also conducted the experiments for the TV t model with $\nu = 1$ in (10) and BS Laplacian model with $\alpha = 100$ in (11), utilizing 10 iterations with the boost start. Although these hyperparameters were the same as those used in [18], the experimental results slightly differed because the settings of the TV Gaussian model, which was employed for the boost start, were modified.

Table VI shows the Δ SDR score for each source model. These scores were averaged over the four scenarios described in Table III. Compared with the TV Gaussian model, we found that the other models yielded better scores and particularly, the TV Laplacian model performed the best. Moreover, considering that the Δ SDR for the TV Gaussian model was the same as that for the other models in the first iteration, we could confirm the iteration effect in the batch SIBF.

C. Comparing Source Models in Online SIBF

Next, we compared the four source models in the online SIBF using the setups described in the second row of Table V. First, employing the TV Gaussian model with $T_b = 5$ s (312 frames) in Algorithm 1, we tuned g and K_{pm} (forgetting factor and iteration count for the PM, respectively). Table VII shows the adopted values and corresponding reasons.

Subsequently, we evaluated the Δ SDR scores for each source model, varying T_b such that $1 \text{ s} \leq T_b \leq 5 \text{ s}$ (62 to 312 frames). For the source models other than the TV Gaussian, we fixed K_{aux} , which is the iteration count for the

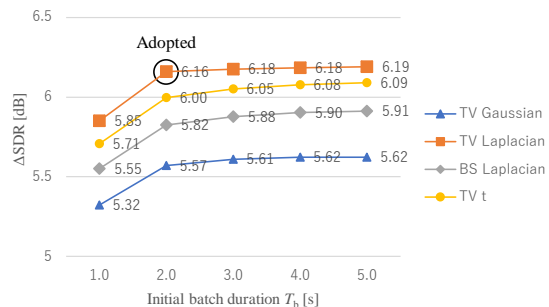


Fig. 6 Relationship between Δ SDR and initial batch duration T_b for each source model in online SIBF; the TV Laplacian model with $T_b = 2$ s was adopted.

auxiliary function algorithm, to 1 in Algorithm 1. The results plotted in Fig. 6 confirmed the following aspects:

- 1) Similar to the batch algorithm, the TV Laplacian model demonstrated the best accuracy.
- 2) The Δ SDR scores were almost constant for $2 \text{ s} \leq T_b \leq 5 \text{ s}$, while they degraded for $T_b = 1 \text{ s}$.
- 3) Compared with the batch algorithm shown in Table VI, the scores were lower for all the source models. The gaps between the algorithms were the maximum for the TV Laplacian model, and slightly less for the TV Gaussian model.

Considering that the latency increases as T_b becomes larger, we adopted the TV Laplacian model with $T_b = 2 \text{ s}$ (125 frames) as the most appropriate setting for the online SIBF.

D. Iteration Effect

For the TV Laplacian model, we evaluated the iteration effects, using the setup described in the third row of Table V. Table VIII shows the results, when K_{aux} in Algorithm 1 was varied between 1 and 10. We found that the iteration slightly lowered the Δ SDR, which is in contrast to that in the batch algorithm. Therefore, we fixed K_{aux} to 1 in subsequent experiments.

E. Scaling methods: MDP vs. SWF

Next, we compared the MDP- and SWF-based scaling methods using the setup described in the fourth row of Table V. To examine the experimental results in detail, we show, in Table IX, the Δ SDR scores for all the scenarios in both the batch and online algorithms. Consequently, we observed the following:

- 1) In scenarios employing MDB-based scaling, the online algorithm demonstrated inferior performance compared with the batch algorithm.
- 2) Substituting MDP-based scaling with SWF-based scaling enhanced the Δ SDR scores across all scenarios for both the online and batch algorithms.
- 3) Utilizing SWF-based scaling, the online algorithm either exceeded or equaled the performance of the batch algorithm, signifying that this substitution had a more

TABLE VIII
EFFECTS OF ITERATION IN ONLINE SIBF USING TV LAPLACIAN MODEL

Iteration	K_{aux}	Δ SDR [dB]
1		6.16
2		6.14
5		6.10
10		6.08

TABLE IX
COMPARISON BETWEEN MDP-BASED AND SWF-BASED SCALING METHODS IN Δ SDR FOR EACH SCENARIO

Scaling	Algorithm	Δ SDR [dB]				Mean
		BG \times 0.25 (least noisy)	BG \times 0.5 (less noisy)	BG \times 1.0 (noisier)	BG \times 2.0 (noisiest)	
MDP	Batch	5.06	7.12	7.60	6.34	6.53
	Online	4.97	6.74	7.02	5.92	6.16
SWF (proposed)	Batch	6.12	9.13	10.80	10.50	9.14
	Online	6.32	9.28	10.83	10.48	9.23

pronounced positive impact on the Δ SDR scores of the online algorithm relative to the batch algorithm.

The third aspect suggests that the SWF-based scaling can eliminate the accuracy gap between the two algorithms.

Here, we explain the difference between the two scaling methods via specific examples in Fig. 7, which consists of six signals, and each of which is approximately 5-s long and represents as both a waveform and spectrogram. Each spectrogram is a close-up of the frequency bins between 100 and 1000 Hz. The parts (a), (b), (c), and (d) in Fig. 7 denote the target, mixture of the interferences, observation, and reference, respectively. The target is the clean speech labeled as *F01_22GC010A*, and includes two silent periods at both edges of the segment, as highlighted on the waveform. The mixture of the interferences is background noise recorded in a bus and includes louder noise components in the frequency bins under 200 Hz, as highlighted on the spectrogram. We refer to them as the lower-frequency noise. The observation is a mixture of the target and interferences and belongs to the BG \times 2.0 scenario in Table III. This also includes the lower-frequency noise; hence, the silent periods appear to be unclear. This signal is also used as the scaling target for the MDP-based scaling. In (d), the lower-frequency noise is removed and the silent periods at both edges can be identified, as highlighted on both the waveform and spectrogram. This signal is also used as the scaling target for the SWF-based scaling.

Fig. 7 (e) and (f) denote the SIBF outputs with the MDP-based scaling (conventional) and SWF-based scaling (proposed), respectively. Each result appears to be influenced by the characteristic of the corresponding scaling target; in (e), the lower-frequency noise remains, and consequently the silent periods appear to be less clear than in either (d) or (f); in (f), however, the lower-frequency noise is removed and the silent periods at both edges can be identified. These

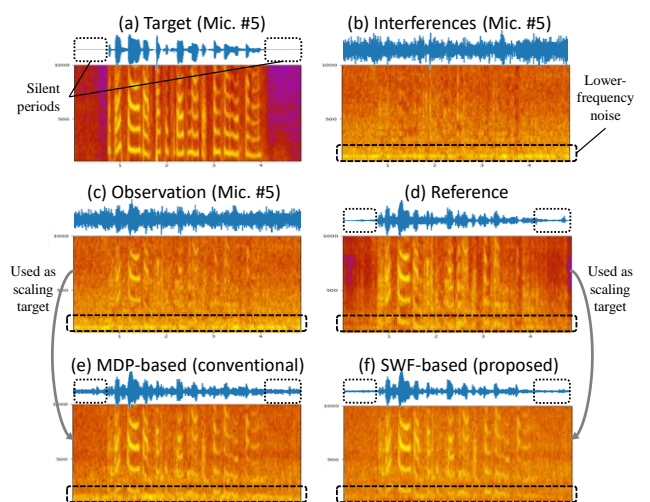


Fig. 7 Waveforms and spectrograms: (a) target, (b) mixture of interferences, (c) observation, (d) reference, (e) SIBF output employing MDP-based scaling (conventional), and (f) SIBF output employing SWF-based scaling (proposed); Results in (e) and (f) utilize (c) and (d), respectively as scaling targets.

differences resulted in the superiority of the SWF-based scaling to the MDP-based scaling.

F. Measuring Latencies

Given that all specifications for the online algorithm had been established, we measured the processing time to calculate the latencies for both the algorithms, using the setup described in the fifth row of Table V. Note that the measured time did not include the reference generation time as mentioned in Section VII.A.2) and that the obtained latencies were estimated.

Fig. 8 illustrates the two types of the latencies:

- 1) Beginning-side latency L_{begin} , which is the duration from the segment beginning to the time when the first frame of the SIBF output is generated.
- 2) End-side latency L_{end} , which is the duration from the segment end to the time when the final frame of the SIBF output is generated.

For a system using the batch algorithm, L_{end} is identical to the duration of the extraction process and L_{begin} is the sum of L_{end} and segment duration T_{seg} . Therefore, the latencies increase as the segment becomes longer. To simplify the estimation, it was assumed that the batch algorithm's processing time for each segment remained constant, irrespective of the T_{seg} .

By contrast, for a system using the online algorithm, both latencies are defined as follows:

$$L_{\text{begin}} = T_b + T_{\text{init}}, \quad (62)$$

$$L_{\text{end}} = \max(L_{\text{begin}} - (1 - F_{\text{rtf}})T_{\text{seg}}, 0), \quad (63)$$

where T_{init} and F_{rtf} denote the duration for the initialization process corresponding to Lines 6 to 9 in Algorithm 1, and real-time factor (RTF), that is, the mean ratio between the processing time and segment duration, respectively. Considering that T_{init} depends on T_b only, L_{begin} is constant. If $F_{\text{rtf}} < 1$, L_{end} can be smaller than L_{begin} and be zero when $T_{\text{seg}} \geq (T_b + T_{\text{init}})/(1 - F_{\text{rtf}})$, whereas L_{end} is maximized when $T_{\text{seg}} = T_b + T_{\text{init}}$.

Table X shows the estimated latencies for both batch and online SIBFs, including the mean and worst-case

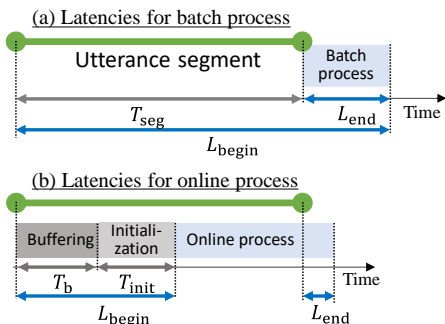


Fig. 8 Definitions of the beginning-side latency (L_{begin}) and end-side latency (L_{end})

(maximum) values. We found that the online SIBF could reduce both L_{begin} and L_{end} in both the values.

Combining the results from Sections VII.E and VII.F, we can infer that the online SIBF has not only reduced the latencies, but also maintained the extraction accuracy.

G. Comparison with Other Methods

In our final experiment, we compared the online SIBF with several conventional methods, such as the online mask-based BF, online ICA-based TSE, and batch SIBF, using the setup described in the bottom row of Table V. This experiment used the CHiME-3 simulated test set and the following performance metrics: the SDR, perceptual evaluation of speech quality (PESQ) [63], short-time objective intelligibility measure (STOI) [64], and extended STOI (eSTOI) [65]. Given that these metrics were determined through comparison with clean speech, they share the characteristic that a signal approximating clean speech yields a higher score.

We assumed that the average latencies between the development and test sets were nearly identical, as Table IV suggests that the mean utterance duration of the test set was almost identical to that of the development set.

As a benchmark of a conventional mask-based BF, we evaluated the MMSE BF [20], [66] in both batch and online algorithms. In the batch algorithm, the BF is formulated as the solution to the following minimization problem:

$$\mathbf{w}_{\text{mmse}}(f) = \arg \min_{\mathbf{w}_{\text{mmse}}(f)} \sum_t |q(f, t) - \mathbf{w}_{\text{mmse}}(f)\mathbf{x}(f, t)|^2, \quad (64)$$

where $\mathbf{w}_{\text{mmse}}(f)$ and $q(f, t)$ denote the extraction filter and a reference signal for the MMSE BF, respectively. Similar to the SWF-based scaling, we compute $q(f, t)$ using (52). Given that $r(f, t)/|x_m(f, t)|$ serves as a TF mask in (52), the MMSE BF utilized in this experiment qualifies as a mask-based BF. In the online algorithm, the extraction filter can be computed as follows:

$$\mathbf{w}_{\text{mmse}}(f, t) = \Phi_x(f, t)^{-1}\varphi_q(f, t), \quad (65)$$

where $\varphi_q(f, t)$ is obtained with (53) and (54). We employed $g = 0.99$ and $T_b = 2$ s (125 frames), which were the same settings as those used in the online SIBF. The MIL was applied to compute $\Phi_x(f, t)^{-1}$ in (65).

The formula for the MMSE BF can be decomposed into MVDR BF and SWF-based scaling (or postfiltering) [20], [59], [66]. Therefore, we can interpret that the MMSE BF

TABLE X
LATENCIES FOR BATCH AND ONLINE SIBFs USING TV LAPLACIAN MODEL
(the smaller the better)

Algorithm	RTF	Mean [s]		Worst [s]		Note
		L_{begin}	L_{end}	L_{begin}	L_{end}	
Batch	0.058	6.72	0.37	14.54	0.37	10 iterations
Online (proposed)	0.070	2.09	0.00	2.09	0.22	$T_b = 2$ s, $T_{\text{init}} = 0.09$ s

TABLE XI
PESQ, SDR, STOI, AND ESTOI SCORES FOR ALL THE METHODS USING THE CHiME-3 SIMULATED TEST SET (KF: KALMAN FILTER)

Method	Algorithm	Source model	Scaling	PESQ	SDR [dB]	STOI [%]	eSTOI [%]
Observation of Microphone #5				2.18	7.54	87.03	68.32
Reference	Batch			2.61	13.61	91.50	78.11
Online SIBF (proposed)	Online	TV Laplacian	SWF	2.75	18.09	96.03	88.30
Batch SIBF	Batch	TV Laplacian	SWF	2.74	17.98	96.11	88.46
Online MMSE BF	Online		(SWF)	2.54	14.41	93.48	81.36
Batch MMSE BF	Batch		(SWF)	2.54	14.54	93.75	81.96
Hiroe 2021 [18] (SIBF with iterative casting)	Batch	BS Laplacian	MDP	2.72	17.29	96.18	
Cho+ 2021 [31] (MLDR BF)	Online	TV t with $\nu = 0$ or TV GG with $\rho = 0$		2.67			85.8
Martín-Doñas+ 2020 [40] (MVDR BF)	Online		KF		14.89		84.1

differs from the SIBF in terms of the filter estimation only, while being identical to it in terms of the scaling.

Table XI presents the scores of the SIBF and MMSE BF for both the online and batch algorithms, in addition to the observation, reference, and those of our previous study [18], online MLDR BF [31], and online MVDR BF [40]. The top two rows correspond to the observation and reference, which are identical to those in our previous study because the same dataset and DNN were employed. The observation SDR is substantively identical to the SNR. As explained in Section V.B, these rows also compare $x_m(f, t)$ and $q(f, t)$ with $m = 5$, which are used as the scaling target for the MDP- and SWF-based methods, respectively, and suggest that the latter is closer to the ideal scaling target $x_{\text{tgt}}(f, t)$, which corresponded to clean speech in the experiments.

The third and fourth rows show the scores of the SIBF for the online and batch algorithms, respectively. These rows demonstrate practically same scores, compared with the first two rows. Therefore, we can infer that in the test set, the online SIBF has also achieved both latency reduction and extraction accuracy maintenance.

The fifth and sixth rows show the scores of the MMSE BF for the online and batch algorithms, respectively. These were obtained in our run. We confirmed that the SIBF outperformed the MMSE BF in all the metrics in both the algorithms, despite using the same reference and scaling method.

The seventh row corresponds to our previous study that employed a technique called iterative casting, which iteratively casts the SIBF output into a DNN to obtain a more accurate reference and output. This row shows the best scores obtained in the sixth casting, albeit incurring approximately six times the computational cost compared with the regular batch algorithm. By contrast, the batch algorithm in this study achieved superior or comparative results without the iterative casting, thanks to the usage of TV Laplacian model and SWF-based scaling.

The bottom two rows correspond to conventional online linear TSE methods, such as the online MLDR [31] and mask-based MVDR BFs [40]. Similar to the online SIBF, these methods update the extraction filter frame by frame and do not use any nonlinear methods in post-process. As mentioned in Sections III.B and VI.B, we regard the source model in [31] as the TV t model with $\nu = 0$ or TV GG model

with $\rho = 0$. In [40], the MVDR BF was combined with the scaling method based on the Kalman filter (KF). The online SIBF outperformed these conventional online methods.

VIII. DISCUSSION

This section discusses the following aspects sequentially:

- A) Primary and side effects in deriving the online algorithm;
- B) Effects of the SWF-based scaling;
- C) Behavior of the TV GG model;
- D) Superiority of the SIBF to the MMSE BF.

A. Primary and Side Effects in Deriving the Online Algorithm

1) Primary Effects: Latency Reduction

The primary effects in deriving the online algorithm are reflected in reducing both L_{begin} and L_{end} ; L_{begin} can be shortened by updating the covariance matrices frame by frame. However, accurately estimating the initial values of these matrices requires a proper duration of the observations [39], [40], and the minimum duration was experimentally found to be 2 s. Therefore, the minimum of L_{begin} was the sum of 2 s and the initialization time, which was 0.09 s on an average.

Meanwhile, to reduce the end-side latency L_{end} calculated in (63), lower F_{rtf} or less computational cost is desirable. The cost of computing the covariance matrices can be reduced by using the FIFO or RLS online algorithm instead of the windowed batch algorithm. Moreover, the cost of computing the GEV in (20) can be reduced by applying the PM and MIL. Consequently, we achieved $F_{\text{rtf}} = 0.070$ and $L_{\text{end}} = 0$ as the mean time.

2) Side effects: Accuracy Degradation

The side effects from deriving the online algorithm manifest as degradation of the extraction accuracy when using the MDP-based scaling. As mentioned in Section IV.B, we consider that the degradation may be caused when deriving the FIFO online algorithm, except for the TV Gaussian model. We discuss this by illustrating the dependencies between the extraction filter and related signals, as shown in Fig. 9.

Fig. 9 (a) shows the TV Gaussian case, which is an exception. The weights $c(f, t - T_b + 1)$ to $c(f, t)$ are computed from (58) and they do not depend on $\mathbf{w}(f, t)$, while they affect $\mathbf{w}(f, t)$ via $\Phi_c(f, t)$. Hence, the FIFO online algorithm is equivalent to the windowed batch algorithm in terms of the extraction accuracy. Considering that the RLS online algorithm approximates the FIFO online algorithm, this should demonstrate almost the same accuracy as the windowed batch algorithm. Comparing Table VI and Fig. 6 for the TV Gaussian model, the gap between the batch and RLS online algorithms is 0.08 dB at minimum. We can interpret that this gap is small and comes from the derivation from the batch to the windowed batch, as shown in Fig. 3, and not that from the windowed batch to the FIFO online.

In contrast, alternative models exhibit distinct dependencies, as depicted in Fig. 9 (b). In the case of the windowed batch algorithm, the weights $c(f, t - T_b + 1)$ to $c(f, t)$ are influenced by $\mathbf{w}(f, t)$ and, conversely, also exert an influence on it. These interdependencies arise from the auxiliary function algorithm discussed in Section VI.B. This algorithm performs alternating minimizations for $\mathbf{w}(f, t)$ and the auxiliary variables [29], [30]. In this study, the latter minimization is included in the computation of weights $c(f, t - T_b + 1)$ to $c(f, t)$ depending on $\mathbf{w}(f, t)$.

The FIFO online algorithm, however, changes the dependencies as illustrated in Fig. 9 (c) because (25) is used instead of (21); only $c(f, t)$ depends on $\mathbf{w}(f, t)$ whereas $c(f, t - T_b + 1)$ to $c(f, t)$ affect $\mathbf{w}(f, t)$. In the context of the auxiliary function algorithm, it can be inferred that the minimization for the auxiliary variables is incomplete; it is complete for $c(f, t)$ only, and not for $c(f, t - T_b + 1)$ to $c(f, t - 1)$. We can consider that the same issue applies to the RLS online algorithm and thus, caused the following behaviors in the experiments:

- 1) The iteration did not improve the extraction accuracy unlike in the batch algorithm, as mentioned in Section VII.D. This is because updating $\mathbf{w}(f, t)$ rarely affects $\Phi_c(f, t)$ in (28).
- 2) As for the models other than the TV Gaussian model, the RLS online algorithm degraded the accuracy to a larger extent, as shown in Table VI and Fig. 6. This is because the online algorithm is no longer equivalent to the original auxiliary function algorithm.

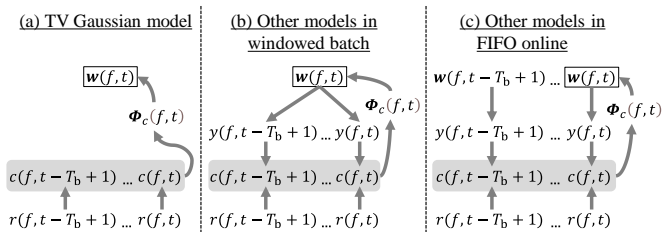


Fig. 9 Dependencies between the extraction filter $\mathbf{w}(f, t)$ and associated signals for (a) the TV Gaussian model in both windowed batch and FIFO online configurations, (b) additional models examined within the windowed batch context, and (c) additional models investigated using the FIFO online approach.

The behavior of the online algorithms derived from the auxiliary function algorithm has not been investigated. Therefore, these findings can contribute to studies that use this algorithm.

B. Effects of the SWF-based Scaling

The experimental results on the SWF-based scaling demonstrated the following trends:

- 1) This scaling method outperformed the MDP-based one in both batch and online algorithms.
- 2) This scaling method appeared to eliminate the accuracy gap between the two algorithms.

Herein, we discuss both the aforementioned aspects. While doing so, we denote the attributes of having a small or large absolute value as simply *small* or *large*.

1) Why the SWF-based Scaling Outperforms the MDP-based Scaling?

Comparing the results presented in Fig. 7 (e) and (f), a salient distinction emerges: the SWF-based scaling successfully eliminates lower-frequency noise present in the observation, while MDP-based scaling does not achieve this. To clarify, frequency bins characterized by lower-frequency noise satisfy that $|x_{\text{tgt}}(f, t)| \ll |x_{\text{itf}}(f, t)|$ in (46), and that the residual interferences $y_{\text{itf}}(f, t)$ described in (47) remain substantial. For MDP-based scaling, the scaling factor within these bins is essentially influenced by the second term of (48) and is thus estimated to be significantly larger than the ideal value denoted in (51). Consequently, this method accentuates residual interferences through the application of a larger scaling factor, causing lower-frequency noise to persist, as observed in Fig. 9 (e).

Contrastingly, the SWF-based scaling method effectively eliminates lower-frequency noise. Experimental outcomes delineated in Section VII.G indicate that the scaling target for SWF-based scaling more closely approximates that of the ideal scaling, as compared to the MDP-based scaling. Consequently, the SWF-based scaling is more akin to ideal scaling, as elaborated in Section V.B.2). The scaling factor for SWF-based scaling, determined via (52) and (50), is notably smaller than that for MDP-based scaling. This facilitates suppression of residual interferences via the application of a diminished scaling factor. In essence, SWF-based scaling enhances the extraction accuracy of the SIBF output by selectively attenuating noisy frequency bins. This corroborative effect was previously documented in reference [59], where SWF was employed to mitigate diffuse noise.

Notably, despite MDP-based scaling's prevalent use in the field of ICA, the issue of its amplification of residual interferences remains unexplored. Therefore, these insights represent a substantive contribution to the field.

2) Why the SWF-based Scaling Can Eliminate the Accuracy Gap?

Table IX suggests that the SWF-based scaling effectively nullified the accuracy gap between the batch and online algorithms, as evidenced by the comparable or superior scores

achieved by the latter. This trend is corroborated by the data in Table XI. It is our assessment that the positive effect of SWF-based scaling is not attributable to the prevention of accuracy degradation in the online algorithm; rather, it functions to obscure the iteration effects present in the batch algorithm.

As mentioned in Sections VII.B and VII.D, the batch algorithm benefits from iterative effects that enhance accuracy, an advantage not shared by the online algorithm. We consider that this enhancement is most pronounced in noisy frequency bins, specifically where $|x_{\text{tgt}}(f, t)| \ll |x_{\text{itf}}(f, t)|$ in (46). This supposition is substantiated by earlier findings that demonstrated more significant improvements noisier environments through iterations [18]. However, the application of SWF-based scaling potentially eliminates these iteration effects, as this technique is adept at attenuating noisy bins. Therefore, SWF-based scaling not only enhances the extraction accuracy in both the batch and online algorithms but also serves to bridge the accuracy gap between both methodologies.

Additionally, Table IX reveals that the online algorithm surpasses the batch algorithm in performance under both the BG \times 0.25 and BG \times 0.5 conditions. The explanation for these findings remains an unresolved issue, as the preceding discussion does not adequately account for this outcome.

C. Behavior of the TV GG Model

Here, we discuss particularly the behavior of the TV Gaussian and Laplacian models, which correspond to the TV GG models with $\rho = 2$ and $\rho = 1$ in (56), respectively. The experimental results in Sections VII.B and VII.C suggest that the TV Laplacian model outperformed the TV Gaussian model in both the algorithms. Given that the online algorithm no longer contains the iteration effects, the results from using this algorithm appear to be remarkable.

Comparing the denominators in (58) and (61), we can interpret that the TV Laplacian model employs a combined value computed from $r(f, t)$ and $y(f, t)$ as a revised reference. In short, if $y(f, t)$ is more accurate than $r(f, t)$, the combined value can work as a more accurate reference than $r(f, t)$ alone; thus, this model can outperform the TV Gaussian model even without the iteration effects. For the online algorithm based on Algorithm 1, we can consider that the above condition is probably satisfied in each frame through the following recursive steps:

- 1) Line 8 in Algorithm 1 indicates that $\mathbf{w}(*, 0)$, which is the initial value of the extraction filter, is computed using the windowed batch algorithm. Thus, this filter can make $y(f, 1)$ more accurate than $r(f, 1)$ as the batch algorithm can.
- 2) Lines 17 and 19 indicate that $y(f, t)$ is computed with $\mathbf{w}(f, t - 1)$ in the case of $K_{\text{aux}} = 1$. If $\mathbf{w}(f, t - 1)$ fits not only the $(t - 1)$ -th frame but also the t -th one, this filter can make $y(f, t)$ more accurate than $r(f, t)$.

If all the sources are stationary, this discussion is reasonable because we can consider that the extraction filter is

practically constant over all frames. However, if sources are moving, whether the TV Laplacian model can outperform the TV Gaussian model remains an open question.

The same discussion can also account for the facts that both the BS Laplacian and TV t models outperformed the TV Gaussian model because both (12) and (13) employ a combined value computed from $r(f, t)$ and $y(f, t)$ as a revised reference. However, why the TV Laplacian model outperforms these two models is an open issue to be discussed.

Additionally, another aspect of the TV Gaussian model needs to be discussed. As mentioned in Section VI.A, the order of the clipping and powering is significant for this model. In contrast to our previous study, the clipping is done before the powering in this study. This order can result in a behavior, wherein a single peak appears when the reference exponent β in (58) is varied; Appendix A indicates that the setting of $\beta = 1/4$ achieved the peak accuracy in a stable manner when the clipping threshold $\varepsilon \leq 10^{-4}$. We also found that the setting of $\beta = 1$ was sensitive to the clipping threshold, although this corresponds to the conventional TV Gaussian model that has extensively been used in the fields of the BSS and ICA-based TSE. These findings can also potentially contribute to both these fields.

D. Superiority of the SIBF to the MMSE BF

The experimental results discussed in Section VII.G suggest that the SIBF outperformed the MMSE BF in both the batch and online algorithms, although the two methods leverage the same reference. Considering that the MMSE BF can be interpreted as the cascade of both the filter estimation based on the MVDR BF and SWF-based scaling [20], [59], [66], the differences in the extraction accuracy only arise from the filter estimation.

As mentioned in Section II.A, the SIBF framework has a characteristic that its output can outperform the reference by leveraging the independence of the sources. In fact, the experimental results support this characteristic.

By contrast, the MMSE BF only approximates the reference in terms of the linear filtering represented in (64). Therefore, the scores for this method are basically similar to those for the reference, although this may appear to be superior or inferior to the reference in some metrics; from Table XI, the MMSE BF appears to outperform the reference in the SDR, STOI, and eSTOI, while underperforming it in the PESQ.

IX. CONCLUSIONS

In this study, we detailed an online method for target sound extraction, referred to as online SIBF, to achieve both latency reduction and maintenance of extraction accuracy, compared with the batch SIBF. By examining techniques used in both online mask-based BF and ICA-based TSE, we derived an online algorithm from the existing iterative batch algorithm. Although this derivation reduced latency, it introduced two challenges: 1) the possibility of reduced extraction accuracy due to changes in the dependencies between the extraction filter and related signals; 2) the potential for

increased accuracy gap between the two algorithms in post-processing, as MDP-based scaling is sensitive to interferences present in both observations and the estimated target.

To address these issues and maintain optimal accuracy, we introduced a new scaling method, referred to as the SWF-based scaling. This method uses a reference combined with the observation phase as the scaling target. As a result, this method more closely approximates ideal scaling than does MDP-based scaling, thereby minimizing the accuracy gap between the two algorithms.

For improved extraction accuracy, we employed the TV GG model. Based on discussions of source models in our previous study, we modified this model to include both clipping and powering the reference.

To verify if this study can both reduce latency and maintain extraction accuracy, we conducted several experiments using the CHiME-3 dataset. We confirmed that SWF-based scaling improved accuracy in both the batch and online algorithms and also eliminated the accuracy gap between the two, in contrast to MDP-based scaling. For the source model, the TV Laplacian model achieved the best accuracy as a variation of the TV GG model.

Estimating the latencies for generating the SIBF output, the online algorithm reduced latencies on both the beginning and end sides. Therefore, by combining the online algorithm and SWF-based scaling, we could both reduce latencies and maintain extraction accuracy.

Our future work includes the following aspects: 1) building a system that operates in real time, indicating that reference generation with the DNN will also be implemented in an online manner; 2) verifying that the TV Laplacian model is superior to other models even in a moving source scenario.

Finally, this study contributes to the BSS and BF fields in the following aspects:

- 1) The accuracy degradation caused in deriving the online algorithm from the iterative one based on the auxiliary function;
- 2) The sensitivity of the MDP-based scaling to the interferences included in both the observations and estimated target;
- 3) The behavior of the TV GG model when varying both the reference exponent and clipping threshold;
- 4) The superiority of the SIBF to the MMSE (or MWF) BF in terms of extraction accuracy.

In summary, we anticipate that this study will stimulate additional research in both the BSS and BF fields.

APPENDIX

A. Hyperparameter Tuning for the TV Gaussian Model

Here, we detail the experiments on hyperparameter tuning for the TV Gaussian model, which is a specific model of the TV GG model with $\rho = 2$ in (56). Fig. 10 shows a plot of the Δ SDR scores when both the reference exponent β for $1/8 \leq \beta \leq 2$ and clipping threshold ε for $10^{-10} \leq \varepsilon \leq 2$ are varied. The results appear to be classified into two types. If $\beta \geq 1/2$, the scores are sensitive to ε . This type includes the

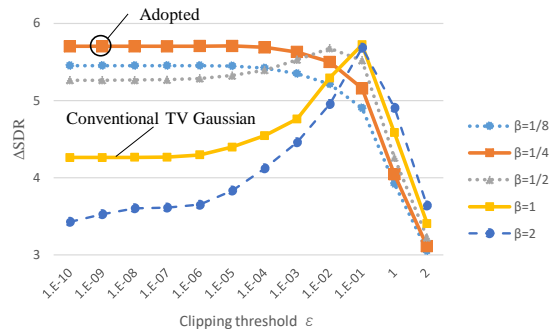


Fig. 10 Relationships between Δ SDR and clipping threshold (ε) across various reference exponent values (β); Adopted parameters include $\beta = 1/4$ and $\varepsilon = 10^{-9}$.

TABLE XII

Δ SDR [dB] FOR THE TV GG MODEL OBTAINED USING DIFFERENT COMBINATIONS OF REFERENCE EXPONENT (β) AND SHAPE PARAMETER (ρ); ADOPTED PARAMETERS INCLUDE $\rho = 1$ AND $\beta = 1/4$

β	ρ			
	1/2	1 (TV Laplacian)	3/2	2 (TV Gaussian)
1/8	6.45	6.46	6.12	5.45
1/4	6.44	6.53	6.30	5.70
1/2	6.34	6.19	5.77	5.26
1	5.98	5.14	4.51	4.26

conventional TV Gaussian model, which corresponds to the case of $\beta = 1$. By contrast, if $\beta \leq 1/4$, the scores were stable for $10^{-10} \leq \varepsilon \leq 10^{-5}$. Given that the latter behavior is more robust to varied hyperparameters, we adopted the parameter set of $\beta = 1/4$ and $\varepsilon = 10^{-9}$ as being the optimal one.

B. Hyperparameter Tuning for the TV GG Model

Next, we detail the experiments of hyperparameter tuning for the TV GG model with $\varepsilon = 10^{-9}$. The estimated targets were obtained with 10 iterations, while the TV Gaussian model was used in the first iteration. Table XII shows the Δ SDR scores for $\rho \in \{1/2, 1, 3/2\}$ and $\beta \in \{1/8, 1/4, 1/2, 1\}$, including those of the TV Gaussian model in the right-most column. We adopted the parameter set of $\rho = 1$ and $\beta = 1/4$ as being the most optimal.

Additionally, the right bottom cell in Table XII corresponds to the conventional TV Gaussian model. We also found that this score (4.26 dB) was much lower than the best score for this model (5.70 dB).

REFERENCES

- [1] J. Barker, R. Marxer, E. Vincent, and S. Watanabe, "The third 'CHiME' speech separation and recognition challenge: Dataset, task and baselines," in *2015 IEEE Workshop on Automatic Speech Recognition and Understanding, ASRU 2015 - Proceedings*, 2016. doi: 10.1109/ASRU.2015.7404837.
- [2] S. J. Chen, A. S. Subramanian, H. Xu, and S. Watanabe, "Building state-of-the-art distant speech recognition using the CHiME-4 challenge with a setup of speech enhancement baseline," *Proceedings of the Annual Conference of the International Speech Communication Association, INTERSPEECH*, vol. 2018-Sept, pp. 1571–1575, 2018. doi: 10.21437/Interspeech.2018-1262.
- [3] M. Delcroix, K. Zmolikova, K. Kinoshita, A. Ogawa, and T. Nakatani, "Single channel target speaker extraction and recognition with

- speaker beam,” in *ICASSP, IEEE International Conference on Acoustics, Speech and Signal Processing - Proceedings*, 2018. doi: 10.1109/ICASSP.2018.8462661.
- [4] Q. Wang *et al.*, “VoiceFilter: Targeted voice separation by speaker-conditioned spectrogram masking,” in *Proceedings of the Annual Conference of the International Speech Communication Association, INTERSPEECH*, 2019. doi: 10.21437/Interspeech.2019-1101.
- [5] T. Ochiai, M. Delcroix, K. Kinoshita, A. Ogawa, and T. Nakatani, “Multimodal SpeakerBeam: Single channel target speech extraction with audio-visual speaker clues,” in *Interspeech 2019, ISCA: ISCA*, Sep. 2019. doi: 10.21437/interspeech.2019-1513.
- [6] H.-W. Dong, N. Takahashi, Y. Mitsufuji, J. McAuley, and T. Berg-Kirkpatrick, “CLIPSep: Learning Text-queried Sound Separation with Noisy Unlabeled Videos,” in *Proceedings of International Conference on Learning Representations (ICLR)*, 2023.
- [7] M. Mizumachi and M. Origuchi, “Advanced delay-and-sum beamformer with deep neural network,” *22nd International Congress on Acoustics (ICA)*, 2016.
- [8] M. Mizumachi, “Neural Network-based Broadband Beamformer with Less Distortion,” *Proceedings of International Congress on Acoustics (ICA 2019)*, p. 2760, Sep. 2019, [Online]. Available: <https://cir.nii.ac.jp/crid/1050011097181720448>
- [9] J. Heymann, L. Drude, A. Chinaev, and R. Haeb-Umbach, “BLSTM supported GEV beamformer front-end for the 3RD CHiME challenge,” *2015 IEEE Workshop on Automatic Speech Recognition and Understanding, ASRU 2015 - Proceedings*, no. June 2016, pp. 444–451, 2016. doi: 10.1109/ASRU.2015.7404829.
- [10] J. Heymann, L. Drude, and R. Haeb-Umbach, “Neural network based spectral mask estimation for acoustic beamforming,” in *2016 IEEE International Conference on Acoustics, Speech and Signal Processing (ICASSP)*, 2016, pp. 196–200. doi: 10.1109/ICASSP.2016.7471664.
- [11] H. Erdogan, J. Hershey, S. Watanabe, M. Mandel, and J. Le Roux, “Improved MVDR beamforming using single-channel mask prediction networks,” *Proceedings of the Annual Conference of the International Speech Communication Association, INTERSPEECH*, vol. 08-12-Sept, pp. 1981–1985, 2016, doi: 10.21437/Interspeech.2016-552.
- [12] A. Hyvärinen, J. Karhunen, and E. Oja, “ICA by Minimization of Mutual Information,” in *Independent Component Analysis*, 2003. doi: 10.1002/0471221317.ch10.
- [13] J. Cmejla and Z. Koldovsky, “Multi-Channel Speech Enhancement Based on Independent Vector Extraction,” in *2018 16th International Workshop on Acoustic Signal Enhancement (IWAENC)*, Sep. 2018, pp. 525–529. doi: 10.1109/IWAENC.2018.8521330.
- [14] B. J. Cho, J. M. Lee, and H. M. Park, “A beamforming algorithm based on maximum likelihood of a complex Gaussian distribution with time-varying variances for robust speech recognition,” *IEEE Signal Process. Lett.*, vol. 26, no. 9, pp. 1398–1402, Sep. 2019. doi: 10.1109/LSP.2019.2932848.
- [15] T. Nakatani and K. Kinoshita, “Simultaneous denoising and dereverberation for low-latency applications using frame-by-frame online unified convolutional beamformer,” in *Proceedings of the Annual Conference of the International Speech Communication Association, INTERSPEECH*, International Speech Communication Association, 2019, pp. 111–115. doi: 10.21437/Interspeech.2019-1286.
- [16] R. Scheibler and N. Ono, “Independent vector analysis with more microphones than sources,” *IEEE Workshop on Applications of Signal Processing to Audio and Acoustics*, vol. 2019-October, no. 17, pp. 185–189, 2019. doi: 10.1109/WASPAA.2019.8937080.
- [17] A. Hiroe, “Similarity-and-Independence-Aware Beamformer: Method for Target Source Extraction Using Magnitude Spectrogram as Reference,” in *Interspeech 2020, 21st Annual Conference of the International Speech Communication Association, Virtual Event, Shanghai, China, 25-29 October 2020*, H. Meng, B. Xu, and T. F. Zheng, Eds., ISCA, 2020, pp. 3311–3315. doi: 10.21437/Interspeech.2020-1365.
- [18] A. Hiroe, “Similarity-and-Independence-Aware Beamformer With Iterative Casting and Boost Start for Target Source Extraction Using Reference,” *IEEE Open Journal of Signal Processing*, vol. 3, pp. 1–20, 2022. doi: 10.1109/OJSP.2021.3120938.
- [19] T. Taniguchi, N. Ono, A. Kawamura, and S. Sagayama, “An auxiliary-function approach to online independent vector analysis for real-time blind source separation,” in *2014 4th Joint Workshop on Hands-Free Speech Communication and Microphone Arrays, HSCMA 2014*, IEEE Computer Society, 2014, pp. 107–111. doi: 10.1109/HSCMA.2014.6843261.
- [20] J. Malek, Z. Koldovský, and M. Bohac, “Block-online multi-channel speech enhancement using deep neural network-supported relative transfer function estimates,” *IET Signal Proc.*, vol. 14, no. 3, pp. 124–133, May 2020. doi: 10.1049/iet-spr.2019.0304.
- [21] Y. Luo and N. Mesgarani, “Conv-TasNet: Surpassing Ideal Time-Frequency Magnitude Masking for Speech Separation,” *IEEE/ACM Trans Audio Speech Lang Process*, vol. 27, no. 8, pp. 1256–1266, Aug. 2019. doi: 10.1109/TASLP.2019.2915167.
- [22] T. Yoshioka, Z. Chen, C. Liu, X. Xiao, H. Erdogan, and D. Dimitriadis, “Low-latency Speaker-independent Continuous Speech Separation,” *ICASSP 2019 - 2019 IEEE International Conference on Acoustics, Speech and Signal Processing (ICASSP)*. 2019. doi: 10.1109/icassp.2019.8682274.
- [23] K. Matsuoka, “Minimal distortion principle for blind source separation,” in *Proceedings of the 41st SICE Annual Conference. SICE 2002*, Soc. Instrument & Control Eng. (SICE), 2003. doi: 10.1109/sice.2002.1195729.
- [24] D. Kitamura *et al.*, “Generalized independent low-rank matrix analysis using heavy-tailed distributions for blind source separation,” *EURASIP J. Adv. Signal Process.*, vol. 2018, no. 1, pp. 9–11, 2018. doi: 10.1186/s13634-018-0549-5.
- [25] S. Mogami, D. Kitamura, Y. Mitsui, N. Takamune, H. Saruwatari, and N. Ono, “Independent low-rank matrix analysis based on complex student’s t-distribution for blind audio source separation,” in *2017 IEEE 27th International Workshop on Machine Learning for Signal Processing (MLSP)*, 2017, pp. 1–6. doi: 10.1109/MLSP.2017.8168129.
- [26] D. Kitamura, “Nonnegative matrix factorization based on complex generative model,” *Acoust. Sci. Technol.*, vol. 40, no. 3, pp. 155–161, 2019. doi: 10.1250/ast.40.155.
- [27] A. Aiba, M. Yoshida, D. Kitamura, S. Takamichi, and H. Saruwatari, “Noise Robust Acoustic Anomaly Detection System with Nonnegative Matrix Factorization Based on Generalized Gaussian Distribution,” *IEICE Trans. Inf. Syst.*, vol. E104.D, no. 3, pp. 441–449, 2021. doi: 10.1587/transinf.2020EDK0002.
- [28] A. Hyvärinen, J. Karhunen, and E. Oja, “ICA by Maximum Likelihood Estimation,” in *Independent Component Analysis*, 2003. doi: 10.1002/0471221317.ch9.
- [29] N. Ono and S. Miyabe, “Auxiliary-Function-Based Independent Component Analysis for Super-Gaussian Sources,” 2010, pp. 165–172. doi: 10.1007/978-3-642-15995-4_21.
- [30] N. Ono, “Stable and fast update rules for independent vector analysis based on auxiliary function technique,” *IEEE Workshop on Applications of Signal Processing to Audio and Acoustics*, vol. 2, no. 9, pp. 189–192, 2011. doi: 10.1109/ASPAA.2011.6082320.
- [31] B. J. Cho and H.-M. Park, “Convolutional Maximum-Likelihood Distortionless Response Beamforming With Steering Vector Estimation for Robust Speech Recognition,” *IEEE/ACM Transactions on Audio, Speech, and Language Processing*, vol. 29, pp. 1352–1367, 2021. doi: 10.1109/TASLP.2021.3067202.
- [32] N. Makishima *et al.*, “Independent Deeply Learned Matrix Analysis for Determined Audio Source Separation,” *IEEE/ACM Transactions on Audio Speech and Language Processing*, vol. 27, no. 10, pp. 1601–1615, 2019. doi: 10.1109/TASLP.2019.2925450.
- [33] T. Tanaka and M. Shiono, “Acoustic Beamforming with Maximum SNR Criterion and Efficient Generalized Eigenvector Tracking,” in *Advances in Multimedia Information Processing -- PCM 2014*, W. T. Ooi, C. G. M. Snoek, H. K. Tan, C.-K. Ho, B. Huet, and C.-W. Ngo, Eds., Cham: Springer International Publishing, 2014, pp. 373–382.
- [34] M. Kitzka, A. Zeyer, R. Schlueter, J. Heymann, and R. Haeb-Umbach, “Robust Online Multi-Channel Speech Recognition,” in *Speech Communication: 12. ITG Symposium*, Oct. 2016, pp. 1–5. [Online]. Available: <https://ieeexplore.ieee.org/abstract/document/7776205/>
- [35] Y.-H. Tu, J. Du, L. Sun, F. Ma, J. Pan, and C.-H. Lee, “A space-and-speaker-aware iterative mask estimation approach to multi-channel speech recognition in the CHiME-6 challenge,” in *Interspeech 2020, ISCA: ISCA*, Oct. 2020. doi: 10.21437/interspeech.2020-2150.
- [36] T. Higuchi, N. Ito, T. Yoshioka, and T. Nakatani, “Robust MVDR beamforming using time-frequency masks for online/offline ASR in noise,” *ICASSP, IEEE International Conference on Acoustics, Speech and Signal Processing - Proceedings*, vol. 2016-May, pp. 5210–5214, 2016. doi: 10.1109/ICASSP.2016.7472671.

- [37] T. Higuchi, N. Ito, S. Araki, T. Yoshioka, M. Delcroix, and T. Nakatani, "Online MVDR Beamformer Based on Complex Gaussian Mixture Model with Spatial Prior for Noise Robust ASR," *IEEE/ACM Transactions on Audio Speech and Language Processing*, vol. 25, no. 4, pp. 780–793, 2017, doi: 10.1109/TASLP.2017.2665341.
- [38] J. Heitkaemper, J. Heymann, and R. Haeb-Umbach, "Smoothing along Frequency in Online Neural Network Supported Acoustic Beamforming," in *Speech Communication: 13th ITG-Symposium*, unknown, Oct. 2018. Accessed: Dec. 26, 2022. [Online]. Available: <http://dx.doi.org/>
- [39] Y. H. Tu, J. Du, N. Zhou, and C. H. Lee, "Online LSTM-based Iterative Mask Estimation for Multi-Channel Speech Enhancement and ASR," *2018 Asia-Pacific Signal and Information Processing Association Annual Summit and Conference, APSIPA ASC 2018 - Proceedings*, no. November, pp. 362–366, 2019, doi: 10.23919/APSIPA.2018.8659564.
- [40] J. M. Martín-Doñas, J. Jensen, Z.-H. Tan, A. M. Gomez, and A. M. Peinado, "Online Multichannel Speech Enhancement Based on Recursive EM and DNN-Based Speech Presence Estimation," *IEEE/ACM Transactions on Audio, Speech, and Language Processing*, vol. 28, pp. 3080–3094, 2020, doi: 10.1109/TASLP.2020.3036776.
- [41] K. Shimada, Y. Bando, M. Mimura, K. Itoyama, K. Yoshii, and T. Kawahara, "Unsupervised Beamforming Based on Multichannel Nonnegative Matrix Factorization for Noisy Speech Recognition," in *2018 IEEE International Conference on Acoustics, Speech and Signal Processing (ICASSP)*, Apr. 2018, pp. 5734–5738. doi: 10.1109/ICASSP.2018.8462642.
- [42] S.-J. Chern, K.-L. Chang, C.-H. Sun, and R.-H. Huang, "Beamspace approach broadband array beamformer with sliding window LC-RLS algorithm for moving jammer suppression," in *Proceedings of 2004 International Symposium on Intelligent Signal Processing and Communication Systems, 2004. ISPACS 2004.*, Nov. 2004, pp. 545–549. doi: 10.1109/ISPACS.2004.1439116.
- [43] M. Long and W. Xin-yue, "Robust adaptive beamforming based on sliding-window RLS algorithm," in *2010 2nd International Conference on Signal Processing Systems*, Jul. 2010, pp. V3-793-V3-797. doi: 10.1109/ICSPS.2010.5555483.
- [44] J. Yang, H. Xi, F. Yang, and Y. Zhao, "RLS-based adaptive algorithms for generalized eigen-decomposition," *IEEE Trans. Signal Process.*, vol. 54, no. 4, pp. 1177–1188, Apr. 2006, doi: 10.1109/TSP.2005.863040.
- [45] J. Yang, Y. Zhao, and H. Xi, "Weighted rule based adaptive algorithm for simultaneously extracting generalized eigenvectors," *IEEE Trans. Neural Netw.*, vol. 22, no. 5, pp. 800–806, May 2011, doi: 10.1109/TNN.2011.2113354.
- [46] Q.-G. Liu and L.-K. Zou, "Eigenvector method for adaptive interference nulling," in *1991 IEEE International Symposium on Circuits and Systems (ISCAS)*, Jun. 1991, pp. 2794–2797 vol.5. doi: 10.1109/ISCAS.1991.176124.
- [47] T. Tanaka, "Fast Generalized Eigenvector Tracking Based on the Power Method," *IEEE Signal Process. Lett.*, vol. 16, no. 11, pp. 969–972, Nov. 2009, doi: 10.1109/LSP.2009.2027667.
- [48] Z. Koldovský and P. Tichavský, "Gradient Algorithms for Complex Non-Gaussian Independent Component/Vector Extraction, Question of Convergence," *IEEE Trans. Signal Process.*, vol. 67, no. 4, pp. 1050–1064, Feb. 2019, doi: 10.1109/TSP.2018.2887185.
- [49] A. Hiroe, "Solution of Permutation Problem in Frequency Domain ICA, Using Multivariate Probability Density Functions," *Plan. Perspect.*, vol. 601, p. 608, 2006.
- [50] T. Kim, T. Eltoft, and T.-W. Lee, "Independent Vector Analysis: An Extension of ICA to Multivariate Components," in *Independent Component Analysis and Blind Signal Separation, 6th International Conference, [ICA] 2006, Charleston, SC, USA, March 5-8, 2006, Proceedings*, 2006, pp. 165–172. doi: 10.1007/11679363_21.
- [51] I. Lee, T. Kim, and T.-W. Lee, "Complex FastIVA: A Robust Maximum Likelihood Approach of MICA for Convolutional BSS," *Plan. Perspect.*, vol. 625, p. 632, 2006.
- [52] T. Kim, H. T. Attias, S. Y. Lee, and T. W. Lee, "Blind source separation exploiting higher-order frequency dependencies," *IEEE Trans. Audio Speech Lang. Processing*, vol. 15, no. 1, pp. 70–79, 2007, doi: 10.1109/TASL.2006.872618.
- [53] J. Janský, J. Málek, J. Čmejla, T. Kounovský, Z. Koldovský, and J. Žďánský, "Adaptive Blind Audio Source Extraction Supervised By Dominant Speaker Identification Using X-Vectors," in *ICASSP 2020 - 2020 IEEE International Conference on Acoustics, Speech and Signal Processing (ICASSP)*, 2020, pp. 676–680. doi: 10.1109/ICASSP40776.2020.9054693.
- [54] J. Janský, Z. Koldovský, J. Málek, T. Kounovský, and J. Čmejla, "Auxiliary function-based algorithm for blind extraction of a moving speaker," *EURASIP Journal on Audio, Speech, and Music Processing*, vol. 2022, no. 1, pp. 1–16, Jan. 2022, doi: 10.1186/s13636-021-00231-6.
- [55] R. Scheibler and N. Ono, "Fast Independent Vector Extraction by Iterative SINR Maximization," *ICASSP, IEEE International Conference on Acoustics, Speech and Signal Processing - Proceedings*, vol. 2020-May, pp. 601–605, 2020, doi: 10.1109/ICASSP40776.2020.9053066.
- [56] T. Ueda, T. Nakatani, R. Ikeshita, K. Kinoshita, S. Araki, and S. Makino, "Low Latency Online Source Separation and Noise Reduction Based on Joint Optimization with Dereverberation," in *2021 29th European Signal Processing Conference (EUSIPCO)*, Aug. 2021, pp. 1000–1004. doi: 10.23919/EUSIPCO54536.2021.9616119.
- [57] T. Nakatani and K. Kinoshita, "Maximum likelihood convolutional beamformer for simultaneous denoising and dereverberation," in *European Signal Processing Conference, EUSIPCO*, Sep. 2019. doi: 10.23919/EUSIPCO.2019.8902753.
- [58] E. Warsitz and R. Haeb-Umbach, "Blind Acoustic Beamforming Based on Generalized Eigenvalue Decomposition," *IEEE Trans. Audio Speech Lang. Processing*, vol. 15, no. 5, pp. 1529–1539, Jul. 2007, doi: 10.1109/TASL.2007.898454.
- [59] N. Ito, N. Ono, E. Vincent, and S. Sagayama, "Designing the Wiener post-filter for diffuse noise suppression using imaginary parts of inter-channel cross-spectra," in *2010 IEEE International Conference on Acoustics, Speech and Signal Processing*, Mar. 2010, pp. 2818–2821. doi: 10.1109/ICASSP.2010.5496202.
- [60] T. Long, J. Benesty, and J. Chen, "Constrained Wiener gains and filters for single-channel and multichannel noise reduction," in *2016 Asia-Pacific Signal and Information Processing Association Annual Summit and Conference (APSIPA)*, Dec. 2016, pp. 1–5. doi: 10.1109/APSIPA.2016.7820804.
- [61] R. K. Jaiswal, S. R. Yeduri, and L. R. Cenkeramaddi, "Single-channel speech enhancement using implicit Wiener filter for high-quality speech communication," *Int. J. Speech Technol.*, vol. 25, no. 3, pp. 745–758, Sep. 2022, doi: 10.1007/s10772-022-09987-4.
- [62] E. Vincent, R. Gribonval, and C. Fevotte, "Performance measurement in blind audio source separation," *IEEE Trans. Audio Speech Lang. Processing*, vol. 14, no. 4, pp. 1462–1469, 2006, doi: 10.1109/TSA.2005.858005.
- [63] J. G. Beerends, A. P. Hekstra, A. W. Rix, and M. P. Hollier, "Perceptual evaluation of speech quality (PESQ): The new ITU standard for end-to-end speech quality assessment. Part II - Psychoacoustic model," *AES: Journal of the Audio Engineering Society*, vol. 50, no. 10, pp. 765–778, 2002.
- [64] C. H. Taal, R. C. Hendriks, R. Heusdens, and J. Jensen, "An Algorithm for Intelligibility Prediction of Time-Frequency Weighted Noisy Speech," *IEEE Trans. Audio Speech Lang. Processing*, vol. 19, no. 7, pp. 2125–2136, 2011, doi: 10.1109/TASL.2011.2114881.
- [65] J. Jensen and C. H. Taal, "An Algorithm for Predicting the Intelligibility of Speech Masked by Modulated Noise Maskers," *IEEE/ACM Transactions on Audio Speech and Language Processing*, vol. 24, no. 11, pp. 2009–2022, 2016, doi: 10.1109/TASLP.2016.2585878.
- [66] S. Stenzel, T. C. Lawin-Ore, J. Freudenberger, and S. Doclo, "A multichannel Wiener filter with partial equalization for distributed microphones," in *Applications of Signal Processing to Audio and Acoustics (WASPAA), 2013 IEEE Workshop on*, unknown, Oct. 2013, pp. 1–4. doi: 10.1109/WASPAA.2013.6701874.



Atsuo Hiroe (M'11) received his B.S. and M.S. degrees in computer science from Tokyo Institute of Technology (Tokyo, Japan) in 1994 and 1996, respectively.

From 1996 to 2014, he worked at Sony Corporation (Tokyo, Japan), conducting research and development on speech recognition, speech signal processing, and natural language understanding, among others. From 2014 to 2016, he was seconded to the National Institute of Information and Communications Technology (Kyoto, Japan) to study spoken dialog systems. Since 2016, he has been working at Sony Group Corporation, conducting research and development on speech signal processing.